Geological Magazine

www.cambridge.org/geo

Variation of lacustrine carbonate deposition in the Eocene Dongying Depression and its comparison with Holocene environments

Jing Wu[1,2], Chao Liang[3], Renchao Yang[1,2] and Jun Xie[1,2]

[1]School of Earth Science and Engineering, Shandong University of Science and Technology, Qingdao 266590, China; [2]Shandong Province Key Laboratory of Depositional Mineralization & Sedimentary Mineral, Shandong University of Science and Technology, Qingdao, 266590, China and [3]School of Geosciences, China University of Petroleum (East China), Qingdao, 266580, China

Original Article

Cite this article: Wu J, Liang C, Yang R, and Xie J (2022) Variation of lacustrine carbonate deposition in the Eocene Dongying Depression and its comparison with Holocene environments. *Geological Magazine* **159**: 963–980. https://doi.org/10.1017/S0016756822000103

Received: 23 February 2021
Revised: 18 January 2022
Accepted: 6 February 2022
First published online: 30 March 2022

Keywords:
lacustrine carbonate deposition; depositional model; Dongying Depression; Holocene sediments; modern lakes

Author for correspondence:
Jing Wu, Email: wujing6524982@163.com;
Chao Liang, Email: liangchao0318@163.com

Abstract

The sedimentary characteristics and preservation potential of lacustrine carbonates provide fundamental information on climate change. The lacustrine carbonate deposition in the Eocene Dongying Depression was investigated using a combination of mineralogical, petrological and geochemical analyses. Micritic calcite/dolomite, granular calcite, columnar calcite, calcareous shell fragments and reworked detrital calcite were identified. Varying patterns of carbonates (VPC) including lithofacies, geochemical indicators and carbonate distribution were revealed in the Dongying Depression: (i) carbonates hardly precipitate in the nearshore area (average 12 wt %); (ii) carbonate content is high (average 53 wt %) in the shallow lake and (iii) gradually decreases to reach a minimum (average 24 wt %) in the deeper part of the lake. Comparison of VPC in four Holocene lakes (the Qinghai Lake and Barkol Lake in China, Oro Lake in Canada and Montcortès Lake in Spain) with the Dongying Depression suggests that four distinct lake stages were developed, namely the terrigenous clastic/gypsum-rich, carbonate-rich, carbonate-decreasing and carbonate-poor stages. A depositional model of lacustrine carbonates influenced by detrital influx, climate, palaeoproductivity and salinity is developed. This study contributes to the understanding of the genetic mechanisms of lacustrine carbonate deposition to reconstruct environmental changes.

1. Introduction

Lacustrine carbonates are an important inorganic carbon sink (Dean, 1999; Einsele *et al.* 2001; Li *et al.* 2013) because the dissolution and burial of carbonate are crucial aspects of the global carbon cycle (Archer *et al.* 1989; Schrag *et al.* 2013). Carbonate deposition is sensitive to climate change, thus providing a valuable proxy for palaeoclimate reconstruction (Platt & Wright, 1991; Dean & Megard, 1993; Détriché *et al.* 2013). As reservoirs or source rocks, lacustrine carbonates further have a considerable petroleum-geology significance (Katz, 2001; Thompson *et al.* 2015). With the exploration and development of shale oil and gas in recent years (Slatt & Rodriguez, 2012; Zou *et al.* 2013; Zhang *et al.* 2021), studying carbonate-rich shale has become increasingly important (Macquaker & Adams, 2003; Loucks & Stephen, 2007; Kong *et al.* 2017). The depositional mechanism of lacustrine carbonates remains a topic for active research (Last & Vance, 2002; Last & Last, 2012; Lima & Ros, 2019).

Lacustrine carbonates have various sources, including reworked detrital carbonates, chemical precipitation and biological processes (Talbot & Kelts, 1986; Hodell *et al.* 1999; Jiang *et al.* 2007; Singh *et al.* 2017). Carbonate deposition is influenced by many factors, including temperature variations in the water column (Gilbert & Leask, 1981; Bassetti *et al.* 2004), climate (Détriché *et al.* 2013; Nelson & Rey, 2018), water depth (Roeser *et al.* 2016), surface-water plankton (Platt & Wright, 1991; Dean, 1999) and water alkalinity (Shapley *et al.* 2005). Depositional models of lacustrine carbonates have been described in the literature (Platt & Wright, 1991; Gierlowski-Kordesch, 2010; Quijada *et al.* 2013; Lettéron *et al.* 2018). Considerable advances have been made in understanding lacustrine carbonate deposition. However, the varying patterns of lacustrine carbonates and the depositional model based on comparison of the Eocene and Holocene lacustrine carbonates need to be further investigated, in order to deepen understanding of the genetic mechanisms of lacustrine carbonate deposition to reconstruct palaeoenvironmental changes.

The Dongying Depression is a typical representative of faulted basins and is one of the prolific oil-producing basins in eastern China and across Southeast Asia, where more than 30 oilfields have been discovered (Guo *et al.* 2010). Lacustrine carbonates concentrate the organic-rich shale of the Eocene Shahejie Formation, which is a source rock and a target for shale oil exploration and development (Liang *et al.* 2017; Chen *et al.* 2018; Li *et al.* 2018). Nearly 200 m of continuous lacustrine carbonate-rich cores are accumulated, with a carbonate content reaching

CAMBRIDGE UNIVERSITY PRESS

95 wt %. Therefore, the Dongying Depression is an ideal location to study lacustrine carbonate deposition. Carbonate deposition in modern lakes, moreover, provides support for analysing the sedimentary characteristics and controlling factors of carbonate precipitation (Shapley *et al.* 2005; Stephenson *et al.* 2006; Valero-Garcés *et al.* 2014). Based on the analysis of carbonate mineralogy, petrology, geochemistry, vertical evolution and distribution, this study has two objectives: (1) to provide a depositional model of carbonates in the Eocene Dongying Depression and (2) to compare the Eocene and Holocene lacustrine carbonate deposition.

2. Geological setting

2.a. Geological setting of the Dongying Depression

2.a.1. Structural and stratigraphic features

The Dongying Depression is an asymmetric half-graben situated in the southeastern Bohai Bay Basin in eastern China (Fig. 1a—b; Li & Li, 2017). It is bordered by the Chengjiazhuang uplift to the north, the Luxi uplift to the southwest, the Guangrao uplift to the southeast, the Qingtuozi uplift to the northeast, and the Binxian and Qingcheng uplifts to the west. The east–west length and north–south width of the depression are *c.* 90 and 65 km, respectively (Fig. 1c). The depression comprises four oil-bearing sags (Lijin, Boxing, Niuzhuang and Minfeng), a northern steep slope, a central anticline zone and a southern gentle slope (Fig. 1d; Ding *et al.* 2014).

The Dongying Depression hosts Palaeogene, Neogene and Quaternary strata, among which the Palaeogene and Neogene act as the most important basin-filling strata and exhibit a maximum thickness of *c.* 7000 m. The Palaeogene strata include the Kongdian, Shahejie (Es) and Dongying formations from bottom to top (Fig. 2). The Es Formation can be divided into four members (Es1–Es4; Fig. 2; Yang *et al.* 2018). The upper member of Es4 (Es4s) shale is carbonate-rich and was selected for this study.

2.a.2. Sedimentary facies

The Dongying Depression started to expand from the Palaeocene, and the tectonic evolution of the Cenozoic includes three stages: a rifting, a fault–depression conversion and a post-rifting thermal subsidence stage (Fig. 2). The Es4s sub-member was deposited during the rifting stage with a rapid subsidence (~70 m Ma^{-1}; Feng *et al.* 2013; Fig. 2). A semi-deep lake is widely developed in the central area of the basin (Fig. 1c; Tian & Jiang, 2009; Liang *et al.* 2018*b*). Organic-rich shale *c.* 200 m thick is developed in the central area of the Dongying Depression (Fig. 2; Guo *et al.* 2010; Zhang *et al.* 2016). Fan delta and nearshore subaqueous fan are developed along the northern steep slope, and beach-bars are distributed along the southern gentle slope of the Dongying Depression (Fig. 1c; Tian & Jiang, 2009). Sr/Ba and B/Ga ratios suggest that the Dongying Depression is a saline lake of the Es4s sub-member (Liang *et al.* 2018*b*).

2.b. Geological setting of four Holocene lakes

The Qinghai and Barkol lakes in China, the Oro Lake in Canada and the Montcortès Lake in Spain are four Holocene lakes which are comparable to the Dongying Depression and are saline lakes. The sediments in these lakes are rich in carbonates, and the vertical evolution of carbonate deposition is comparable to that of the Dongying Depression.

Qinghai Lake is the largest saline lake in China, spanning an area of 4400 km^2 (Fig. 3a—b; Xu *et al.* 2006; Liu *et al.* 2018). The average water depth is 20 m, with a maximum depth of 27 m (Xu *et al.* 2010). The total organic carbon (TOC) content ranges from 2.25 to 6.80 wt % (average 3.40 wt %; Xu *et al.* 2006). The carbonate content of surface sediments ranges from 30 to 66 wt % (Qian & Song, 2010; Liu *et al.* 2018). It is composed mainly of aragonite and calcite with multiple sources (Qian & Song, 2010; Liu *et al.* 2018). The clay minerals are mainly illite, followed by chlorite, with minor content of montmorillonite and kaolinite (Zeng *et al.* 2014). The content and morphology of carbonate and clay minerals in Qinghai Lake are comparable with those in the Dongying Depression, whereas the terrigenous clastic content is lower. Barkol Lake is a saline lake located in a graben in Xinjiang, China (Fig. 3c–d; Zhong *et al.* 2012). The carbonate content of surface sediment ranges from 6 to 60 wt % (Li *et al.* 2008; Zhao *et al.* 2010). The Oro lake is located in Canada and is a small saline lake (0.5 km^2 and ~30 parts per thousand salinity) with a relatively shallow water body (mean depth 3 m; maximum depth:6 m; Fig. 3e–f; Last & Vance, 2002). Carbonate deposition is dominated by aragonite, calcite and dolomite (Last & Vance, 2002). The Montcortès Lake is located in Spain and is one of the deepest karst lakes in the Iberian Peninsula (Valero-Garcés *et al.* 2014). Montcortès Lake is meromictic, and its water bodies lack mixing, yielding the formation of a permanently anoxic monimolimnion below 18 m in summer and 20 m in winter (water depth up to 30 m; Fig. 3g–h; Corella *et al.* 2011, 2012; Valero-Garcés *et al.* 2014). Calcite laminae textures are developed (4.77–0.26 m) in distal facies, reflecting seasonal changes in limnological conditions (Valero-Garcés *et al.* 2014).

3. Methods

3.a. Data

The data include a composite core of 465 m from wells FY1, LY1 and NY1 in the Dongying Depression (Fig. 1). X-ray diffraction (XRD) was performed on 377 samples, and thin-section observations were performed on 193 samples. Field-emission scanning electron microscopy (FESEM) was performed on 58 samples, X-ray fluorescence (XRF) and inductively coupled plasma – mass spectrometry (ICP-MS) were conducted on 138 samples, and Rock-Eval pyrolysis was performed on 93 samples. All measurements were performed at the Geological Science Research Institute of Shengli Oilfield, Sinopec, except for the FESEM observation, which was performed at the Experimental Research Center of the Petroleum Geology Institute (Wuxi), Sinopec.

Data on mineralogy, petrology and organic geochemistry of the four Holocene lakes were collected from the literature. The chronology of sediment sequence in the four Holocene lakes is derived from radiocarbon ages obtained from accelerator mass spectrometry (Last & Vance, 2002; Li *et al.* 2008; An *et al.* 2012; Valero-Garcés *et al.* 2014). The above data are integrated and discussed with the data from Dongying Depression to analyse the depositional characteristics of lacustrine carbonates.

3.b. XRD and petrology

Mineral and petrological characteristics were obtained using XRD analysis, thin-sections and FESEM observations. Approximately 150 g of fresh rock was pulverized to obtain a sediment fraction finer than 200-mesh size. The XRD analysis was performed on the powdered samples using an X'Pert-Multipurpose Diffractometer. Thin-sections were observed using a polarizing Zeiss microscope (Axio Scope A1). The FESEM observation samples were gold-coated and observed using a HITACHI S-4800 system.

https://doi.org/10.1017/S0016756822000103 Published online by Cambridge University Press

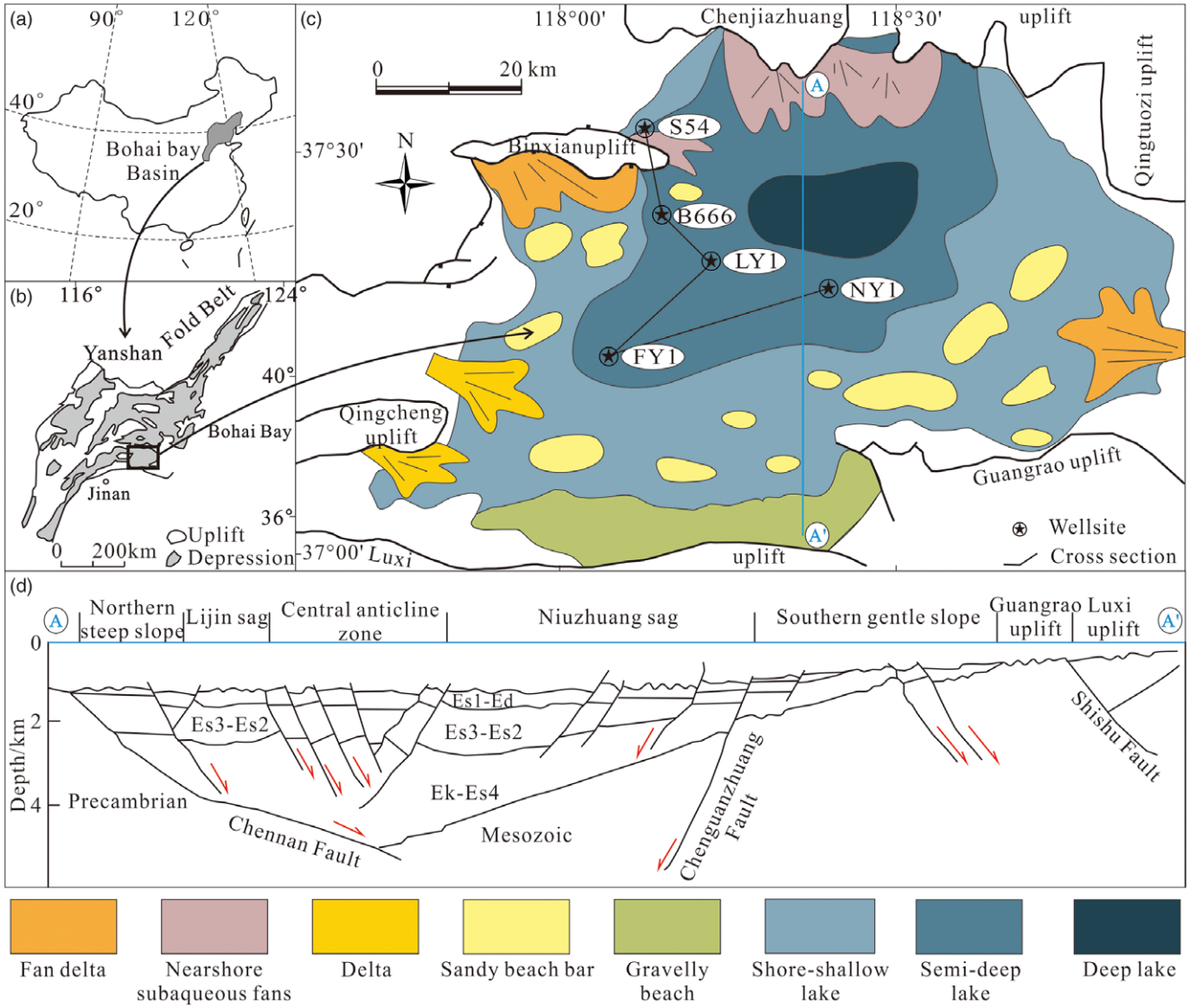

Fig. 1. (Colour online) Location map, structural units and sedimentary facies in the Dongying Depression. (a–b) Location of the Dongying Depression. (c) Sedimentary facies distribution of the Es4s sub-member (Tian & Jiang, 2009). Micropalaeontological analysis suggests that the depth range of shallow lake is 0–15 m and the depth range of semi-deep lake to deep lake is 20–30 m (Su *et al.* 2012). (d) Structural cross-section (for the location, see (c)).

3.c. TOC and Rock-Eval pyrolysis

Analysis of the organic geochemistry characteristics included the TOC, free hydrocarbons (S1, mg HC/g rock), hydrocarbons cracked from kerogen (S2, mg HC/g rock), chloroform bitumen 'A', maximum yield temperature of pyrolysate (T_{max}) and hydrogen index (HI). The TOC content was measured using a CS344 carbon–sulfur detector (Leco Company, US). The Rock-Eval pyrolysis was conducted using the Rock-Eval 6 analyser.

3.d. Assessment of the depositional conditions

The depositional conditions of the Es4s shale were studied based on the analyses of mineralogy, petrology, organic characteristics and inorganic geochemical elements. XRF was performed to determine the major elements (i.e. Na and Al). Trace elements (i.e. Ti, Sr, Ba, V and Ni) were determined via ICP-MS (JY38S).

Titanium (Ti) was used as an indicator for detrital influx (Murphy *et al.* 2000; Tribovillard *et al.* 2006). Relatively low Na/Al ratios are interpreted as intense rainfall and chemical weathering under a warm and humid climate, and conversely indicate predominantly mechanical weathering under arid and cold climate conditions (Aplin, 1993). Therefore, Na/Al ratios can be used as an indicator of the palaeoclimate and strength of chemical weathering. The Sr/Ba ratio can be used as a proxy for water-body salinity because these are positively proportional to each other (Liang *et al.* 2018*b*). Biogenic Ba (Ba_{bio}) is used as a proxy for effective palaeoproductivity and correlates positively to palaeoproductivity (Tribovillard *et al.* 2004). It is usually calculated using the equation $Ba_{bio} = Ba_{tot} - (Al_{tot} \times Ba/Al_{alu}) = Ba_{tot} - (Al_{tot} \times 0.0075)$, where Ba_{tot} and Al_{tot} refer to the total Ba content and total Al content, respectively (Tribovillard *et al.* 2004). Ba/Al_{alu} indicates the Ba/Al ratios of aluminosilicate detritus in crustal rocks, which is commonly set to 0.0075 (Dymond *et al.* 1992). Vanadium (V) tends to be fixed in sediments with organic compounds, and nickel (Ni) frequently precipitates as sulphides under anoxic conditions (Arthur & Sageman, 1994). The V/(V + Ni) ratio positively correlates to reducibility (Arthur & Sageman, 1994; Algeo & Ingall, 2007). In a strongly reducing environment, uranium (U) exists

https://doi.org/10.1017/S0016756822000103 Published online by Cambridge University Press

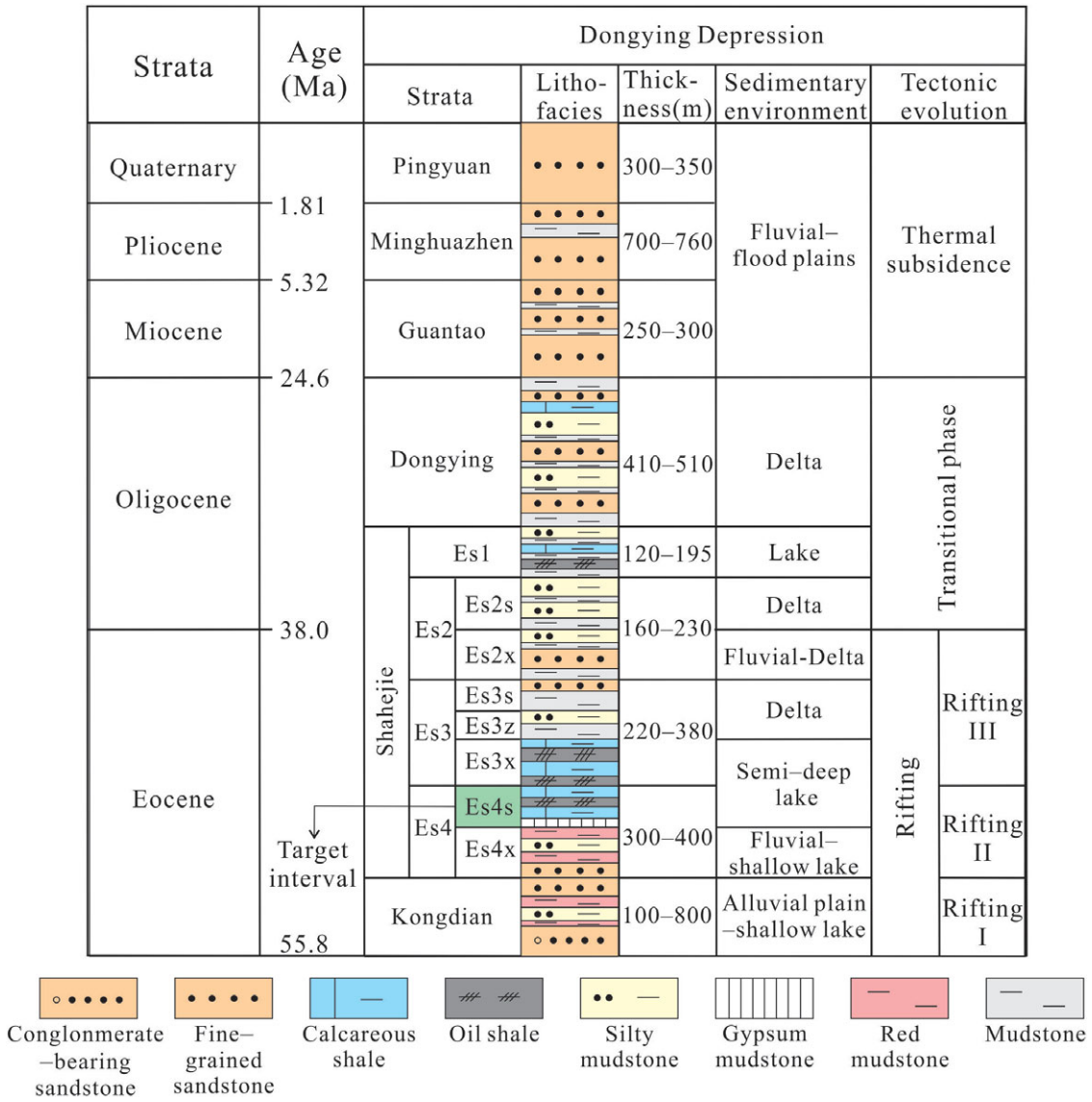

Fig. 2. (Colour online) Stratigraphy of the Dongying Depression (Ma *et al.* 2016; Liang *et al.* 2018*b*).

in the form of insoluble U^{4+}, enhancing the enrichment of U in sediments, whereas it exists in the form of soluble U^{6+} under oxidizing conditions. Thorium (Th) enrichment is not affected by the redox conditions of water bodies. Th/U ratio is a good indicator of redox conditions of bottom water, and correlates negatively to reducibility. (Davies & Elliot, 1996; Zhang *et al.* 2016).

4. Results

4.a. Mineralogy of the Es4s shale in the Dongying Depression

The Es4s sub-member predominantly comprises carbonate, clay minerals and quartz (Fig. 4a). Subordinate pyrite and feldspar were observed. The carbonate content (ranging from 3 to 95 wt % with an average of 51 wt %) mainly comprises calcite (ranging from 1 to 78 wt % with an average of 38 wt %) and dolomite (ranging from 1 to 93 wt % with an average of 14 wt %). The clay mineral content ranges from 2 to 57 wt % (average 16 wt %), with few samples exceeding 50 wt %. The clay minerals are mainly illite, followed by an illite–smectite mixed layer with trace chlorite. The quartz content ranges from 2 to 60 wt % with an average of 24 wt %. The clay mineral content and quartz content both show negative correlations with carbonate content (Fig. 4b–c).

Three major carbonate forms occur, including micritic calcite/dolomite, granular calcite and columnar calcite. The micritic calcite/dolomite is made up with light laminae ranging in thickness from 60 to 400 μm (Fig. 5a–b), interlaced with dark laminae comprising clay minerals and trace organic matter (OM). The micritic calcite recrystallizes to granular calcite, which recrystallizes to columnar calcite as the degree of recrystallization increases (Fig. 5c–f; Liu *et al.* 2017; Bai *et al.* 2018; Liang *et al.* 2018a). Granular calcite has a large particle size (5–20 μm in diameter) and can form light laminae alone or be distributed at the bottom of the micritic calcite laminae (Fig. 5c–d). The laminae comprising columnar calcite are bright and appear alternately with clay lamina enriched in OM (Fig. 5e). The maximum growth orientation of the columnar calcite particles is perpendicular to the laminae deposition plane. In addition, two subordinate forms of carbonate, including calcareous

https://doi.org/10.1017/S0016756822000103 Published online by Cambridge University Press

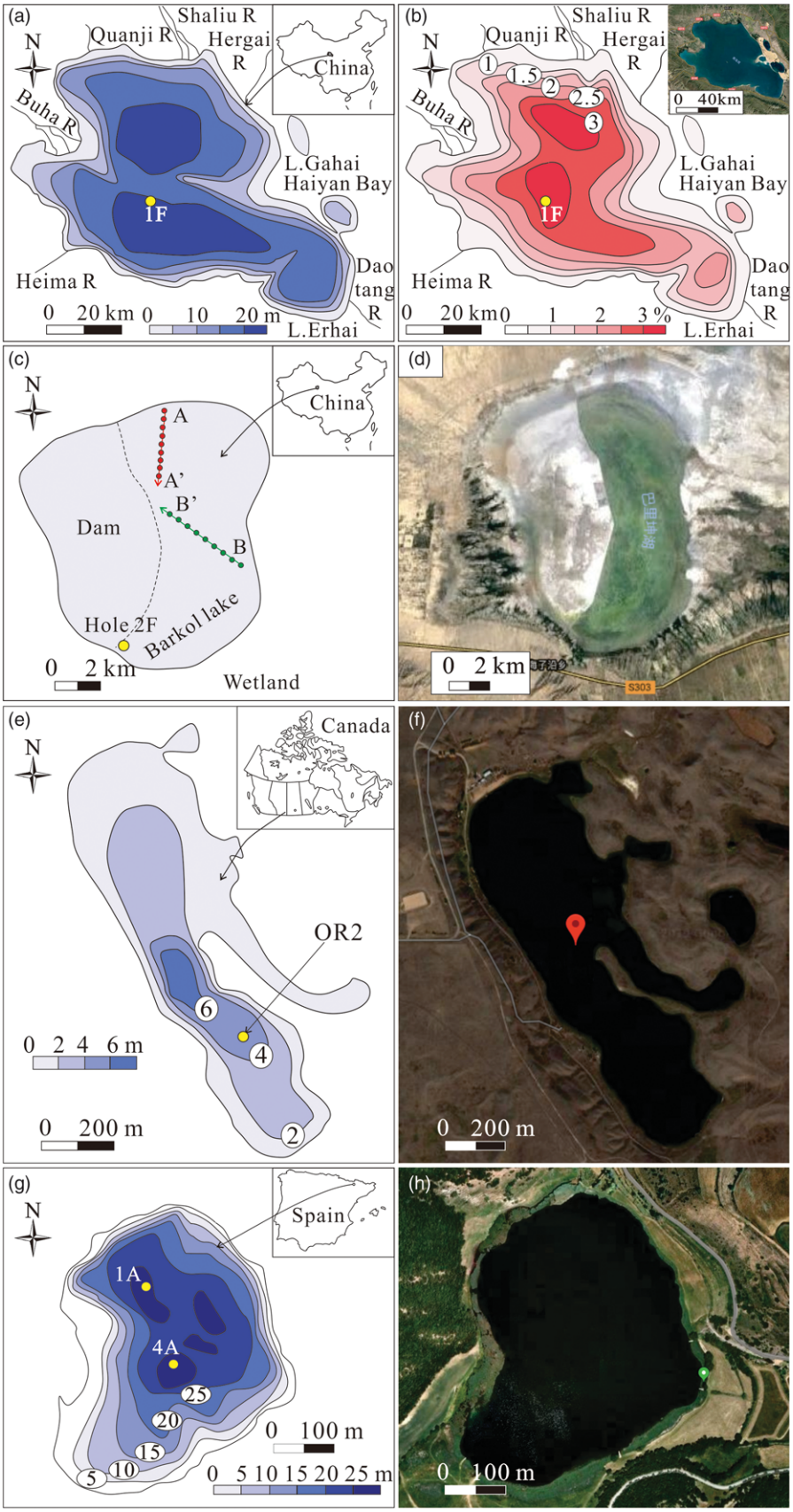

Fig. 3. (Colour online) Geological settings of four modern lakes. (ab) Contour map of water depth and TOC content in Qinghai Lake, respectively, modified from Liu *et al.* (2017) and Huang (1981). (c) Location of Barkol Lake, modified from Li *et al.* (2008). (d) Satellite image of Barkol Lake. (e) Location and bathymetry map of Oro Lake, modified from Last & Vance (2002). (f) Satellite image of Oro Lake. (g) Location and bathymetry map of Montcortès Lake, modified from Valero-Garcés *et al.* (2014). (h) Satellite image of Montcortès Lake.

https://doi.org/10.1017/S0016756822000103 Published online by Cambridge University Press

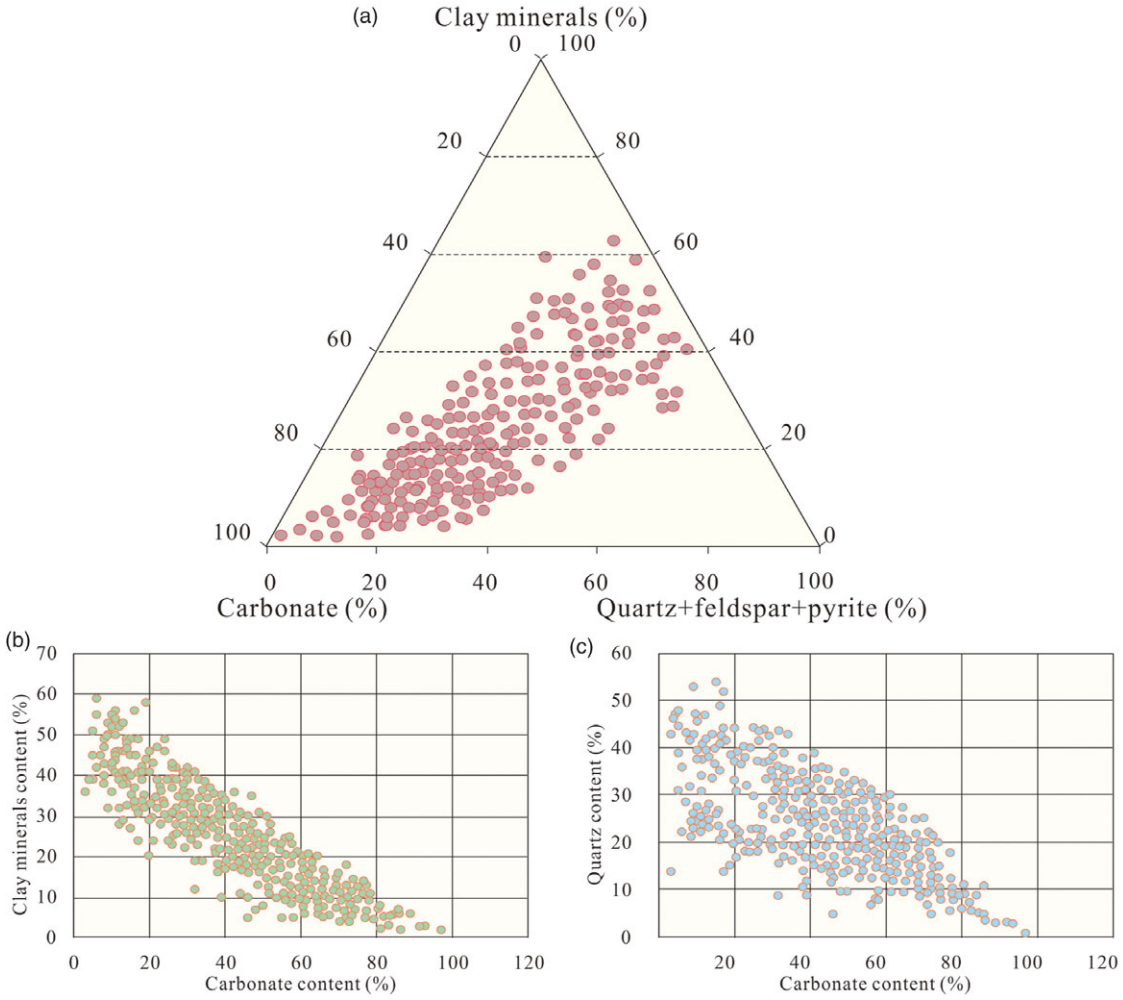

Fig. 4. (Colour online) Ternary diagram of the mineral composition (a) and crossplots of carbonate content vs clay mineral content (b) and quartz content (c) of the Es4s submember in the Dongying Depression.

shell fragments and reworked detrital calcite, occur occasionally (Fig. 5g). The clay minerals are mostly mixed with OM to form dark laminae (Fig. 5b–e). The quartz particles have a sub-angular shape showing the characteristics of a terrigenous origin (Fig. 5h).

4.b. Geochemistry characteristics of the Es4s shale in the Dongying Depression

The Na/Al ratio varies between 0.08 and 0.29 (average 0.14), and the Ba_{bio} content ranges from 58.1 to 845.8 μg g^{-1} (average 433.7 μg g^{-1}). The Ti content ranges from 0.05 % to 0.55 %, with an average of 0.21 %, and the Sr/Ba ratio is high, in the range 1.27–12.80 (average 4.30). The V/(V + Ni) ratio ranges from 0.30 to 0.99, with an average of 0.75 (Fig. 6a). The Th/U ratio ranges from 0.35 to 5.85 (average 1.50), and its vertical variation trend is opposite to the vertical variation trend of the V/(V + Ni) ratio and TOC content (Fig. 6a).

The TOC content ranges from 0.11 to 9.05 wt % (average 2.21 wt %; Fig. 6a). The S1 values range between 0.02 and 6.04 mg g^{-1} (average 2.48 mg g^{-1}), and the S2 values range from 0.01 to 41.08 mg g^{-1} (average 6.81 mg g^{-1}; Fig. 6a). The chloroform bitumen 'A' content is primarily between 0.28 and 0.97, with an average of 0.58. The T_{max} value ranges from 384 °C to 461 °C (average 447 °C), and the HI value ranges from 9.09 to 453.92 mg HC (hydrocarbons)/g TOC (average 296.04 mg HC/g TOC; Fig. 6a). Based on the HI and T_{max}, the OM types are classified and dominated by type-II and type-II–III kerogen, with a few samples characterized by type-III–II and type-III kerogen. The vertical variation trends of S1, S2, chloroform bitumen 'A', T_{max} and HI are similar to that of TOC content (Fig. 6a).

4.c. Petrology of the Es4s shale in the Dongying Depression

According to mineral compositions, TOC content (low TOC: TOC < 2 wt %; middle TOC: 2 wt % < TOC < 4 wt %; high TOC: TOC > 4 wt %) and sedimentary structures, seven lithofacies are identified, namely: (i) grey-blue siltstone; (ii) grey-blue low-TOC massive claystone; (iii) low-TOC laminated limestone; (iv) middle-TOC laminated limestone; (v) high-TOC laminated limestone; (vi) middle-TOC carbonate–silt–clay mixed shale (middle-TOC MS); and (vii) oil shale (Fig. 5). The grey-blue siltstone is characterized by the development of cross-bedding, massive bedding, ripple bedding and bioturbation. The siltstone is developed with a certain degree of hydrodynamism and may be of beach-bar or delta front deposition. The grey-blue low-TOC massive claystone, along with siltstone, only develops at the bottom of the Es4s

https://doi.org/10.1017/S0016756822000103 Published online by Cambridge University Press

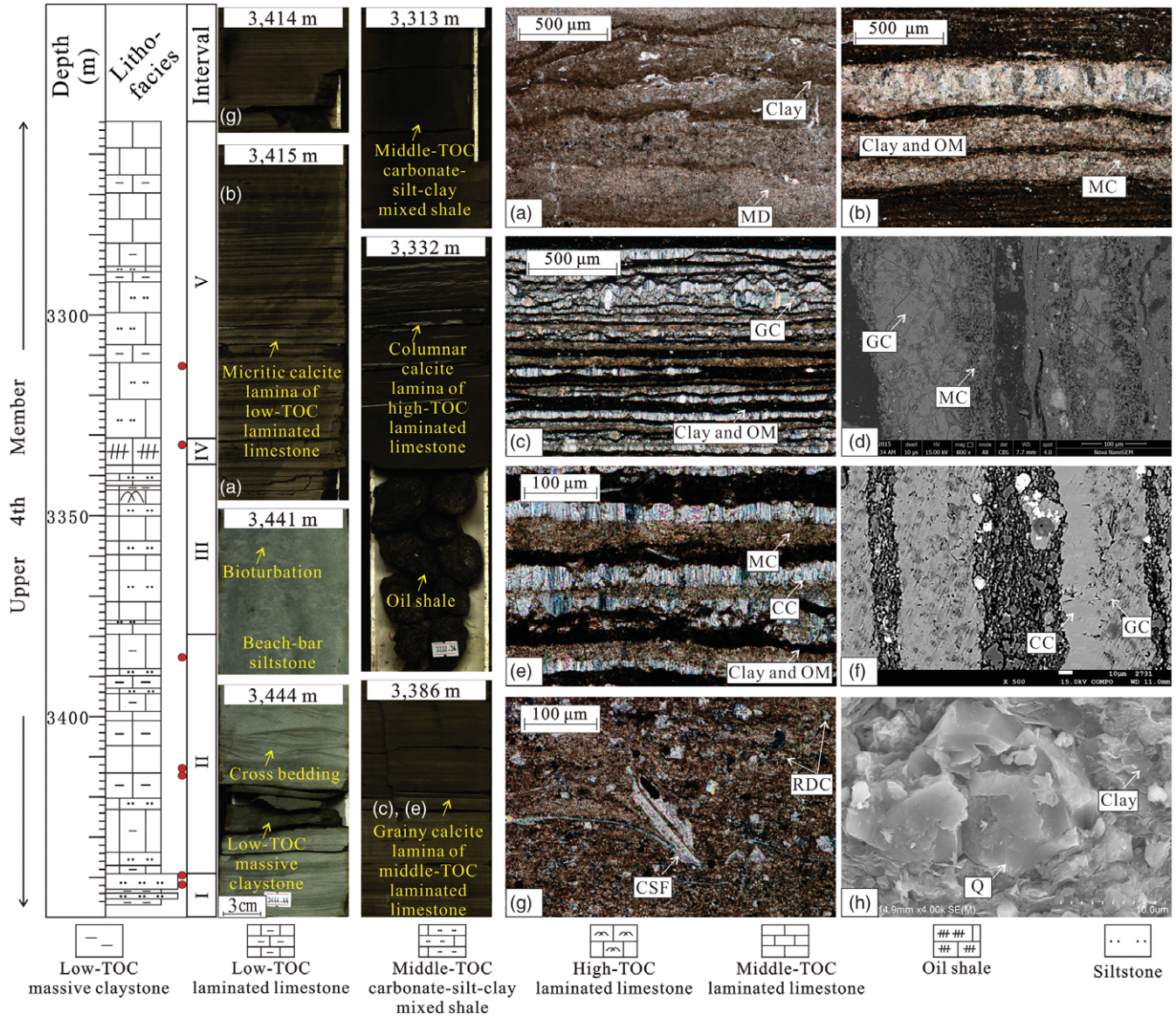

Fig. 5. (Colour online) Macroscopic and microscopic observations of minerals and lithofacies of the Es4s sub-member in the Dongying Depression. The location of samples in the core is marked by the red circle. (a) Light laminae comprise micritic dolomite (MD), Well FY1, 3415 m. (b) Micritic calcite (MC) in low-TOC laminated limestone, Well FY1, 3415 m. (c) Granular calcite (GC) constitutes light laminae, Well FY1, 3386 m. (d) Recrystallization from MC to GC, Well NY1 (Fig. 1c), 3453 m. (e) High-TOC laminated limestone; light laminae comprise columnar calcite (CC), and dark laminae comprise clay minerals and OM, Well FY1, 3386 m. (f) Recrystallization from GC to CC, Well NY1 (Fig. 1C), 3442 m. (g) Reworked detrital calcite (RDC) particles with certain abrasion and a diameter between 5 and 20 μm form massive bedding together with calcareous shell fragments (CSF) and clay minerals, Well FY1, 3414 m. (h) FESEM image showing quartz (Q) surrounded by clay minerals, Well FY1, 3308 m.

sub-member with high clay mineral content (greater than 50 wt %). Based on the aforementioned characteristics of mineral compositions, texture, sedimentary structures, TOC content, lithofacies and sedimentary facies distribution (Fig. 1c), the co-development of these two types of lithofacies indicates a nearshore area. Low-TOC laminated limestone, middle-TOC laminated limestone and high-TOC laminated limestone are commonly carbonate-rich (greater than 50 wt %) lithofacies and are characterized by well-developed laminae suggesting a weak influence of terrigenous input and hydrodynamism. The light laminae of these three lithofacies comprise micritic, granular and columnar calcite, respectively. The dark laminae mainly contain clay minerals and OM. With the increase in TOC content, the core colour of these three lithofacies darkens from grey to black, suggesting a gradual deepening of the water body. Middle-TOC MS is developed in the upper part of the Es4s sub-member and differs from middle-TOC laminated limestone by a relative increase in terrigenous material (e.g. quartz and feldspar), indicating a shallow environment. The average content of quartz and feldspar is 32 wt %. The average content of carbonate decreases to 42 wt %. The clay mineral content ranges from 11 to 35 wt % (average 22 wt %). Oil shale is mainly developed in deep lake, suggested by the black colour in the core, high content of TOC (greater than 4 wt %), and lack of terrigenous material.

4.d. Vertical sedimentary evolution in the Dongying Depression

Based on mineral composition, lithofacies and geochemical data, five intervals (I, II, III, IV and V) are determined from the bottom to the top of the Es4s sub-member.

https://doi.org/10.1017/S0016756822000103 Published online by Cambridge University Press

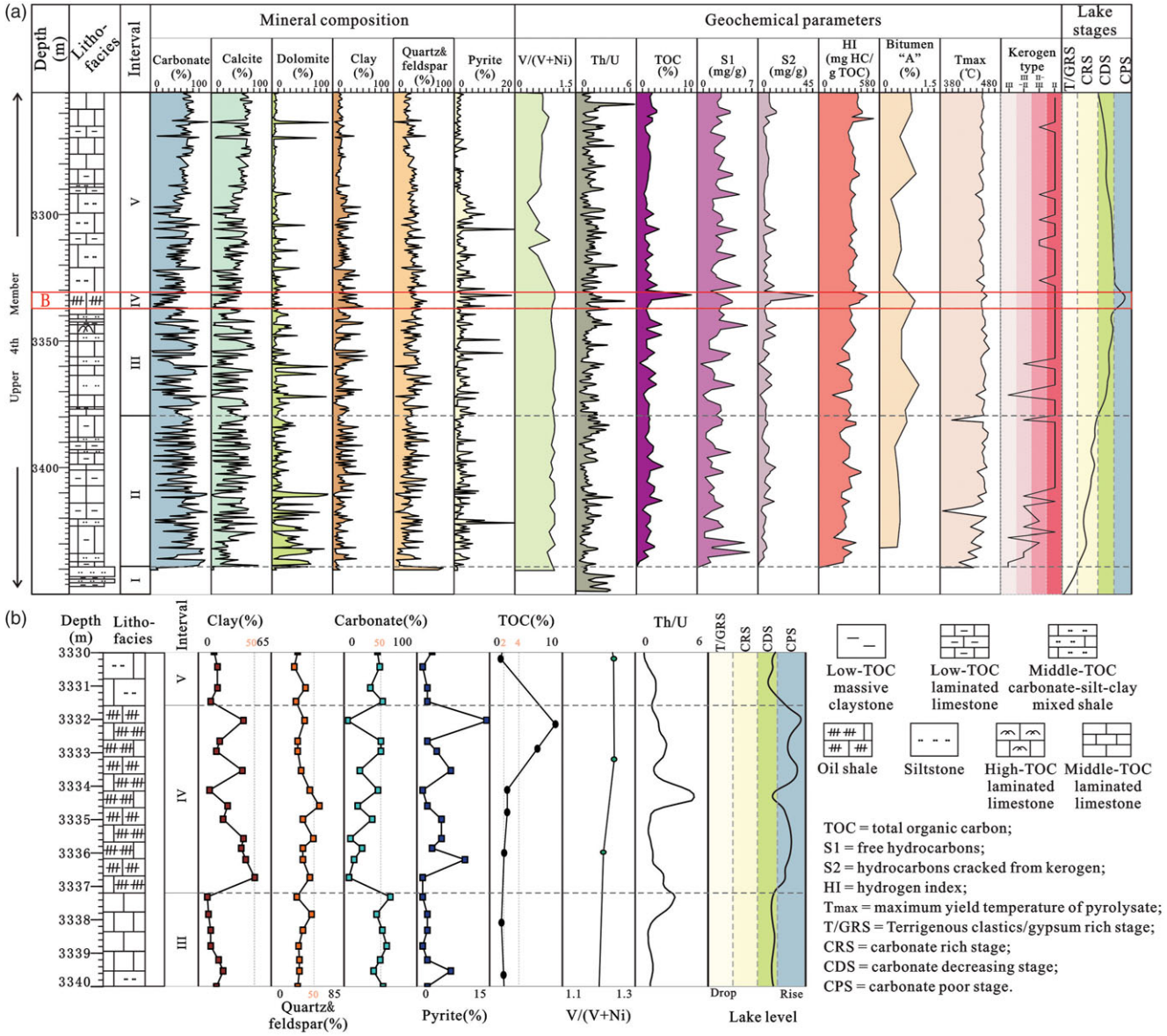

Fig. 6. (Colour online) Vertical evolution (a) and relatively low carbonate content interval (b) of the Es4s sub-member in Well FY1 in the Dongying Depression.

Interval I (3447–3439 m). The lithofacies are dominated by low-TOC massive claystone and siltstone with cross-bedding and intense bioturbation (Fig. 5). The carbonate content and TOC content are the lowest (averages 12 and 0.11 wt %, respectively; Figs 6a and 7) in the entire Es4s sub-member. In contrast, the Th/U ratio is high and increases upward. The aforementioned characteristics suggest that sediments influenced by the terrigenous input in this interval were deposited in the nearshore area (Jiang *et al.* 2011).

Interval II (3439–3380 m). A large amount of carbonate developed in this interval (Figs 6a and 7a). Although the carbonate content frequently fluctuates, it mostly exceeds 50 wt % (Fig. 6a). The average contents of calcite and dolomite reach a maximum. The content of quartz and clay minerals is low (Fig. 6a). The lithofacies is dominated by low-TOC laminated limestone, interlaced with middle-TOC laminated limestone and middle-TOC MS. The content of TOC (average 2.25 wt %) as well as pyrite and the V/(V + Ni) ratio (average 0.93) increases (Figs 6a and 7b), which are all positively proportional to reducibility; these are accompanied by a drastic decrease in Th/U ratio compared with that of interval I. These characteristics suggest that the water body deepened.

Interval III (3380–3337 m). The carbonate content greatly fluctuates, ranging from 3 to 94 wt %, with an average of 48 wt % (Figs 6a and 7a). Low-carbonate-content samples appear at 3356–3359 and 3364–3372 m. The average contents of calcite and dolomite decrease to 33 % and 15 %, respectively. The dominant lithofacies changes from low-TOC laminated limestone of shallow lake facies in interval II to middle-TOC MS and middle/high-TOC laminated limestone of semi-deep lake facies in interval III. The high content of TOC and pyrite, as well as the V/(V + Ni) ratio (ranging from 0.89 to 1.00, average 0.96), suggest that the water body continued to deepen.

Interval IV (3337–3332 m). The carbonate content considerably decreases, ranging from 3 to 49 wt %, with an average of 24 wt % (Fig. 7b). The average calcite and dolomite contents decrease to

https://doi.org/10.1017/S0016756822000103 Published online by Cambridge University Press

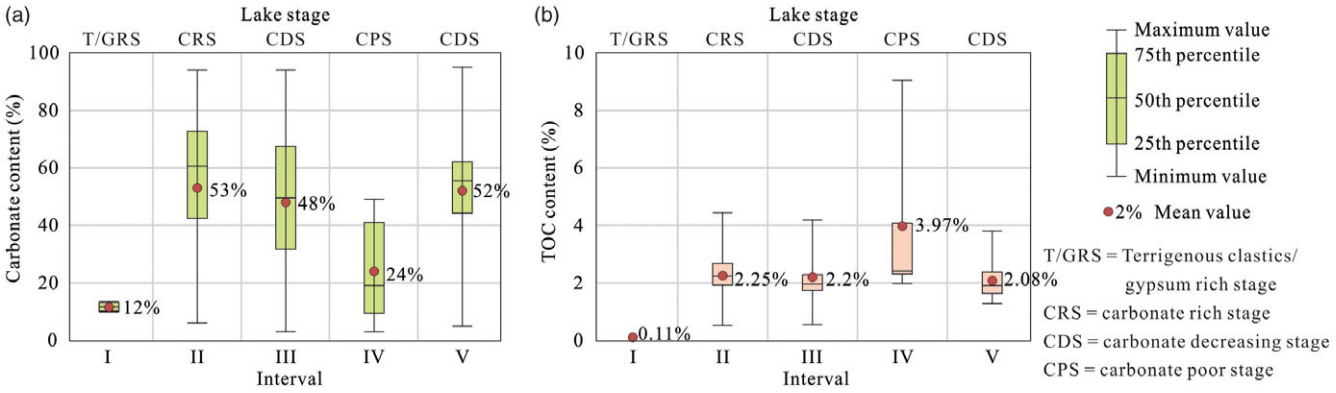

Fig. 7. (Colour online) Contents of carbonate (a) and TOC (b) in five intervals of the Es4s sub-member in the Dongying Depression.

their lowest value (19 and 6 wt %, respectively). The TOC content is the highest (maximum 9.05 wt %, average 3.97 wt %) in the entire Es4s sub-member, and oil shale of deep-lake facies is developed. The V/(V + Ni) ratio and pyrite content reach a maximum, indicating the deepest water level (Fig. 6b). These characteristics suggest that the carbonate content decreases to a minimum in the deep lake.

Interval V (3332–3252 m). The carbonate content increases again (Fig. 6a), ranging from 5 to 95 wt % (average 52 wt %). The average values of calcite and dolomite increase to 44 and 8 wt %, respectively. The dominant lithofacies changes from middle-TOC MS to low-TOC laminated limestone. The Th/U ratio starts to increase, and the TOC content (ranging from 1.29 to 3.79 wt %, average 2.08 wt %), V/(V + Ni) ratio (ranging from 0.31 to 0.98, average 0.63) and pyrite content are all lower than those in interval IV, suggesting a shallowing trend of the water body.

4.e. Distribution of carbonate and lithofacies in the Dongying Depression

Based on the seismic data, well log data and core observations, the Es4s sub-member is interpreted as one entire third-order sequence (Fig. 8, SQ1; Tian & Jiang, 2009; Zahid *et al.* 2016), including the lowstand system tract (LST), transgressive system tract (TST) and highstand system tract (HST). According to the cross-section within the sequence-stratigraphic framework, the distributions of carbonate content and lithofacies were analysed (Fig. 8). Affected by strong terrigenous input, the carbonate content of interval I (LST) is low. Conglomerates are developed in the northern steep slope (Fig. 8, Well S54; Li *et al.* 2019), and siltstone and low-TOC massive claystone with a small amount of gypseous claystone are developed in the central area of the basin (Fig. 8, Well NY1). Throughout interval II (early TST), the dominant lithofacies is sandstone and claystone in the northern basin edge, whose lateral distribution is limited and changes rapidly. The central area of the basin is far away from the sediment input. The lithofacies is dominated by low-TOC laminated limestone with a few thin layers of middle-TOC MS (Fig. 8, Well FY1). Variations in the lithofacies association and high values of TOC, pyrite and V/(V + Ni) ratio indicate that the water body deepens during interval III. The dominant lithofacies changes from siliciclastics in the northern basin edge to middle-TOC MS and middle-TOC laminated limestone toward the centre of the basin. During interval IV (late TST), with the deepening of the water body, the carbonate content considerably decreases in the central basin (Fig. 8; Well LY1, FY1 and NY1). However, the carbonate content increases in the low-TOC laminated limestone of the north basin (Fig. 8, Well B666). Sandstone (Fig. 8, Well S54), claystone, low-TOC laminated limestone (Fig. 8, Well B666), middle-TOC MS (Fig. 8, Well LY1) and oil shale (Fig. 8, Well FY1 and NY1) are successively developed from the edge to the centre of the basin as the water body deepens. In interval V (HST), the change in carbonate content and lithofacies from the edge to the centre of the basin is similar to interval III.

Based on the aforementioned details, carbonates hardly precipitate in the nearshore area, where sedimentation is dominated by terrigenous inputs. However, the carbonate content is high in the shallow lake, where the influence of terrigenous input is reduced and the lithofacies is dominated by low-TOC laminated limestone. As the water body deepens, the carbonate content gradually decreases and the deposition mainly comprises middle-TOC laminated limestone and high-TOC laminated limestone. The carbonate content is minimal in the deep lake, where the lithofacies is dominated by oil shale.

5. Discussion

5.a. A comparison of the Eocene and Holocene lacustrine carbonate deposition

5.a.1. Vertical evolution of lacustrine carbonates

The varying patterns of carbonates (VPC) and sedimentary environments of four modern lakes are investigated based on their lithofacies, mineral content, TOC content and grain size.

Hole 1F was drilled in the deposition centre of the southwestern sub-basin of Qinghai Lake (An *et al.* 2012). We divided the sediments retrieved from hole 1F into four intervals in this study: I, II, III and IV (Fig. 9). The sediments of interval I (18.61–6.68 m) change from khaki fine sand to silt and silty mud. The carbonate content is low, whereas the quartz content is obviously higher than in the other intervals. The TOC flux content is less than 1 g cm^{-2} kyr^{-1}. The mean grain size of this interval is the largest, ranging from 6 to 75 μm (average 36 μm). The low TOC flux content and large grains of sediments suggest that the water body is shallow in this interval (Roeser *et al.* 2016), which may be affected by the arid and cold climate during the last glacial episode (Yu & Kelts, 2002; An *et al.* 2012). In interval II (6.68–5.22 m), grey silty mud is well developed. The carbonate content abruptly increases (*c.* 50 wt %) as a result of aragonite precipitation. The TOC flux content considerably increases to 3 g cm^{-2} kyr^{-1}, which indicates

https://doi.org/10.1017/S0016756822000103 Published online by Cambridge University Press

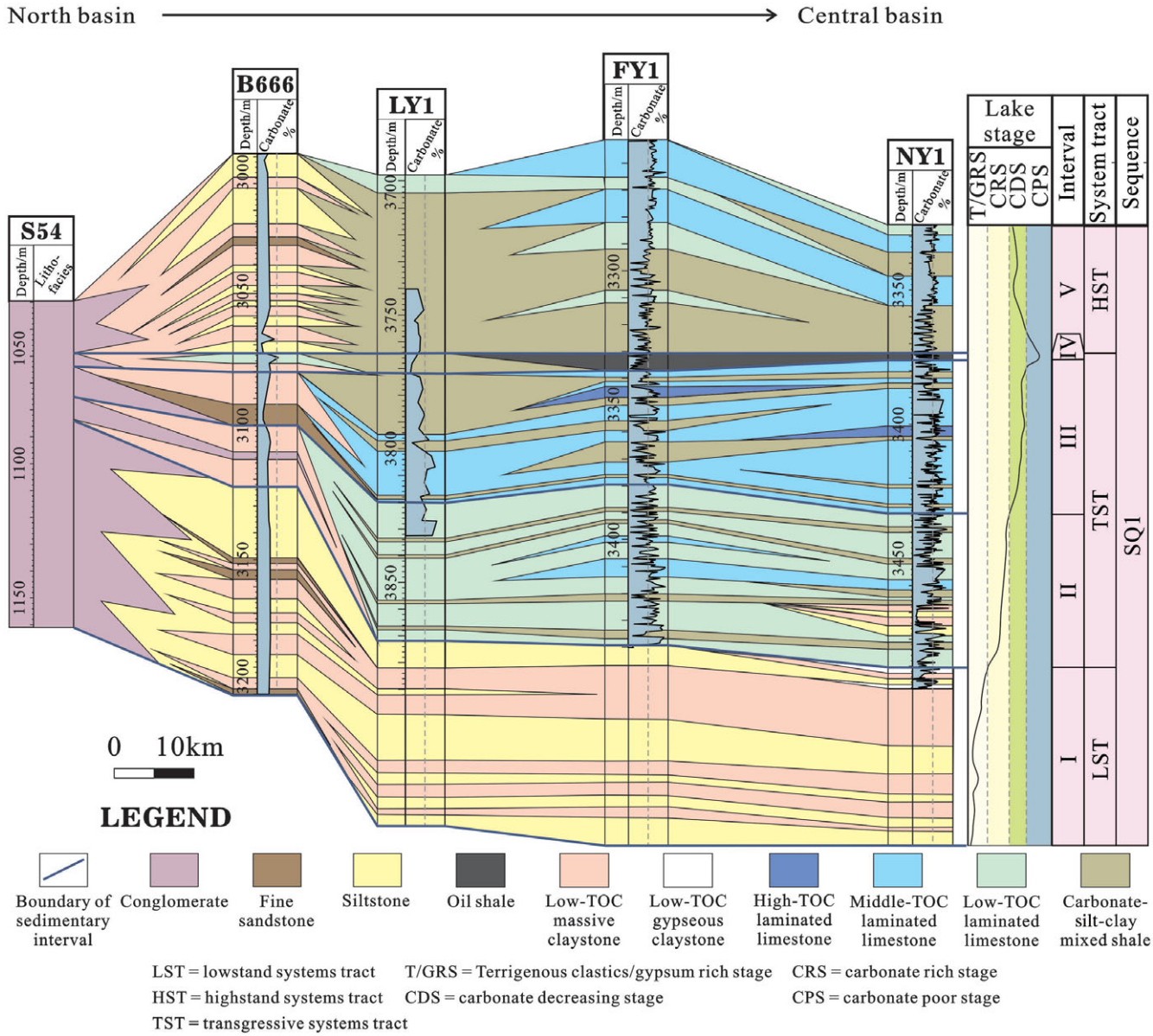

Fig. 8. (Colour online) Lithofacies cross-section of the Es4s sub-member in the Dongying Depression. See Figure 1c for the location of the cross-section.

a deepening water body, combined with the variation in lithology and grain size. The sediments in Qinghai Lake are relatively coarse, and the water body is shallower with stronger terrigenous clastic input compared with the Dongying Depression. The VPC and variation in water body in intervals I and II (18.61–5.22 m) in Qinghai Lake are similar to those of intervals I and II recorded in the Dongying Depression (Figs 6 and 9). The sediments of interval III (5.22–3.78 m) change from light-grey silty mud to grey silty mud, with decreasing grain size. Compared with interval II, even though the content of aragonite and dolomite increases in interval III, the total carbonate content decreases. The TOC flux content remains at a stable, high value (*c.* 3 g cm^{-2} kyr^{-1}). Black-grey mud is dominant in interval IV (3.78–0 m). Both quartz content and mean grain size are low (*c.* 10 wt % and 16 μm, respectively). The water depth is at the maximum, and the carbonate content continues to decrease and then stabilizes, with a high TOC flux content. The VPC in intervals III and IV are similar to those of intervals III and IV in the Dongying Depression, both of which show a deepening water body, decreased carbonate content and smaller sediment grain sizes compared with those of intervals I and II.

Similar VPC are developed in Barkol Lake and Oro Lake (Figs 10 and 11), the sediments of which are divided into five and three intervals in this study, respectively. The carbonate content is low in interval I due to the presence of sandy/gypseous sediments. The amount of carbonate increases abruptly in interval II and decreases in interval III with a deepening water body, as inferred by an enrichment in OM. The carbonate content remains low in interval IV with the deepest water body, as indicated by the minimum sediment grain size, while it increases again in interval V.

The VPC, which are comparable to the Dongying Depression, appear in the sediments of Montcortès Lake (Figs 3g and 12). The water body gradually shallows (intervals III–V) after a short deepening (intervals I and II), which is influenced by the basin

https://doi.org/10.1017/S0016756822000103 Published online by Cambridge University Press

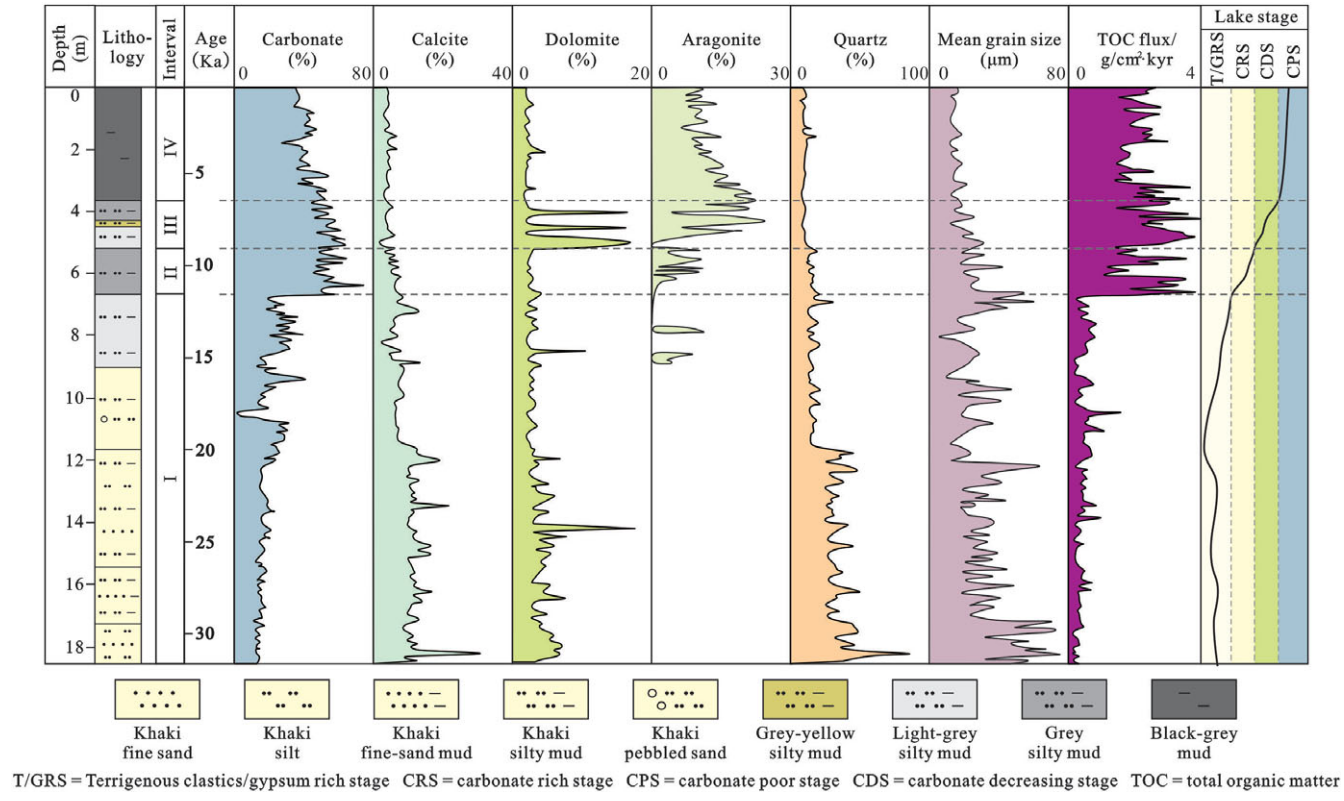

Fig. 9. (Colour online) Vertical evolution of Holocene deposition in hole 1F in Qinghai Lake, modified from Qian & Song (2010) and An *et al.* (2012).

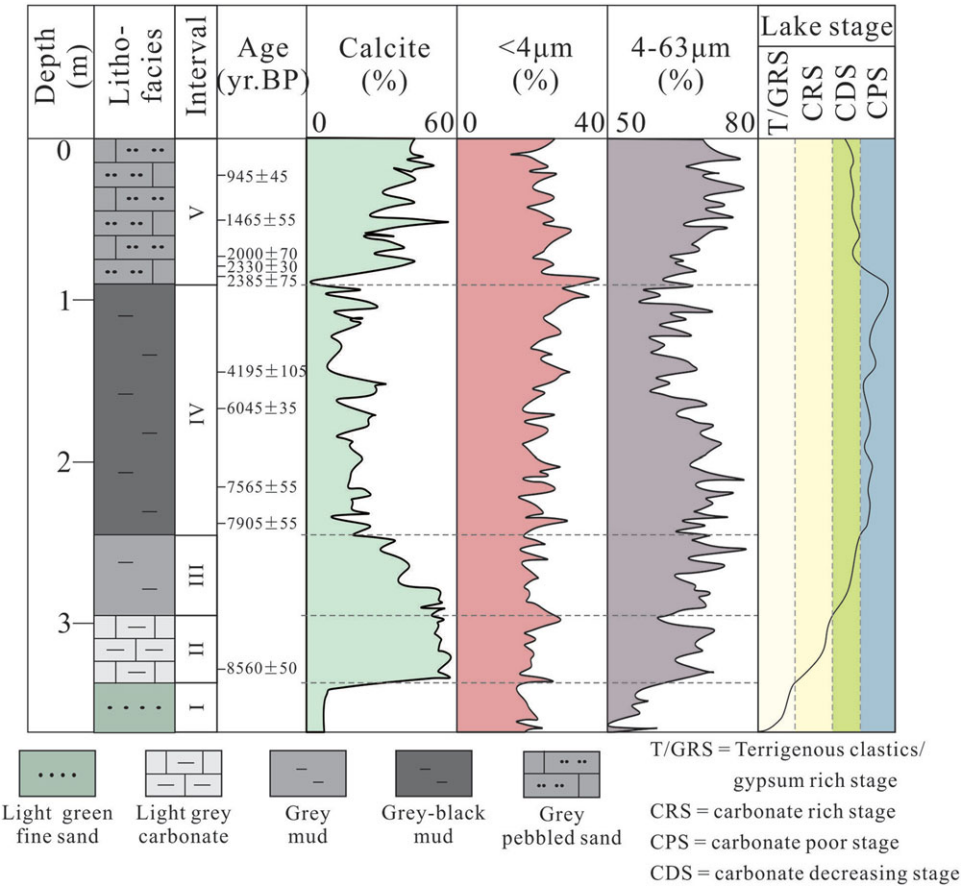

Fig. 10. (Colour online) Holocene deposition in hole 2F in Barkol Lake, modified from Li *et al.* (2008).

https://doi.org/10.1017/S0016756822000103 Published online by Cambridge University Press

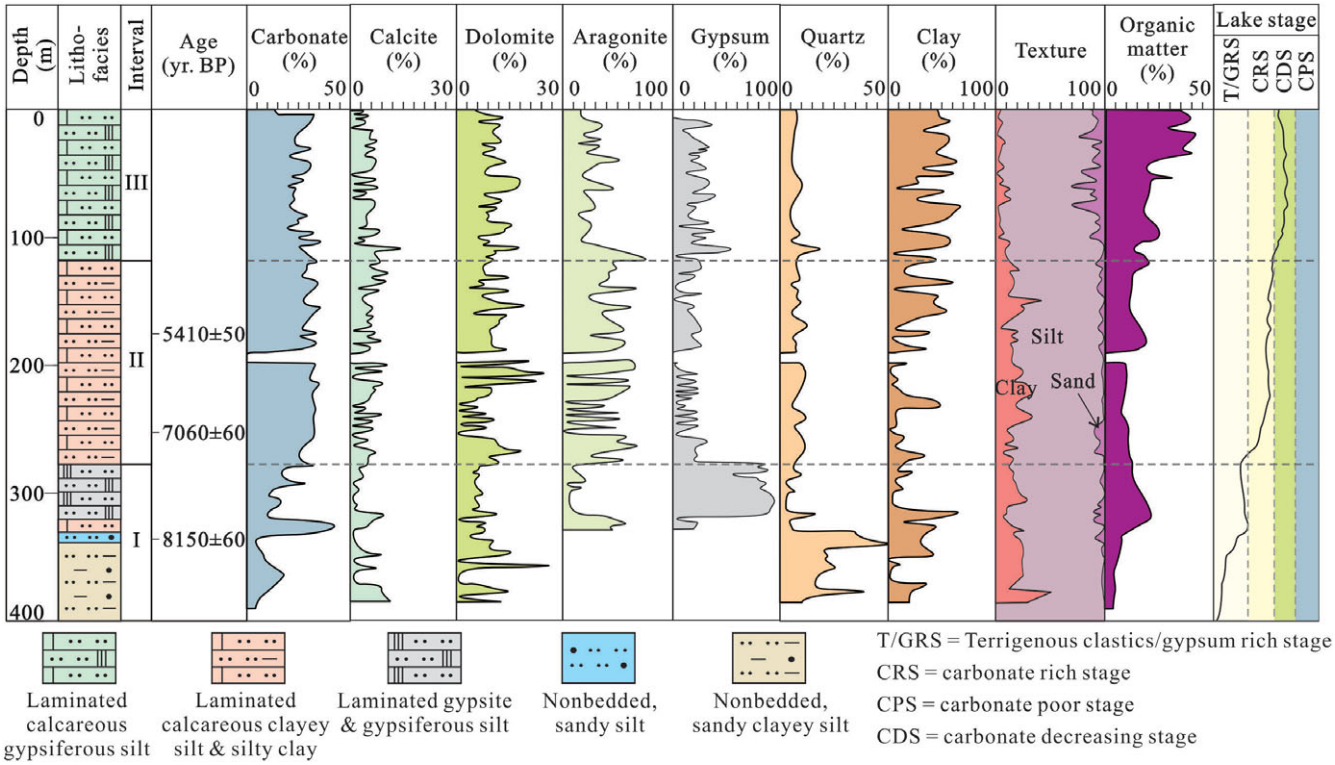

Fig. 11. (Colour online) Content and texture characteristics of sediments in OR2 in Oro Lake, modified from Last & Vance (2002).

morphology, hydrologic fluctuations and climate (Valero-Garcés *et al.* 2014). The water body then shallows again (interval VII) after a slight deepening (interval VI). Correspondingly, the carbonate content is low in intervals I and II, and then gradually increases in intervals III–V. The amount of carbonate decreases in interval V and slightly increases in intervals VI and VII before decreasing again. Although the sequence of sediments differs from the Dongying Depression, the correspondence between carbonate deposition and sedimentary environment is consistent.

5.a.2. Distribution of lacustrine carbonates

The evolution of carbonate content from the basin edge to the centre in the north–south and southeast–northwest directions in Barkol Lake is illustrated in Figure 13 (Zhao *et al.* 2010). Taking the transect BB′ as an example, the carbonate content increases from 21 wt % at BB′1 to 32 % at BB′7 and decreases to 19 wt % at BB′9 at the basin centre (Fig. 13b). The lateral distribution of the Holocene deposition shows that the carbonate content gradually increases to a maximum from the edge of the basin to its centre and then decreases at the deepest water zone, which is consistent with VPC in the Dongying Depression (Figs 6a and 8).

5.b. Genetic mechanisms of variation in carbonate

According to the VPC and sedimentary environment, four distinct lake stages are determined: terrigenous clastic / gypsum-rich stage (T/GRS), carbonate-rich stage (CRS), carbonate-decreasing stage (CDS) and carbonate-poor stage (CPS), corresponding to intervals I, II, III and IV, respectively.

T/GRS (Interval I): The terrigenous input is strong, as indicated by the high content of Ti, which enhances the enrichment of silt, hindering carbonate precipitation (Figs 8, 14 and 15; Bomou *et al.* 2013; Montero-Serrano *et al.* 2015). Simultaneously, gypsum is developed by evaporation under an arid climate condition in some areas lacking terrigenous clastic (Fig. 8, Well NY1; Liang *et al.* 2018*b*).

CRS (Interval II): The terrigenous input greatly decreases, reducing the dilution effect of terrigenous materials and providing suitable conditions for carbonate precipitation. Based on the evaporative setting in interval I, a decreasing Na/Al ratio and a high Sr/Ba ratio indicate a warm climate and salinized water body in interval II. Such depositional conditions favour the chemical precipitation of calcite (Last & Vance, 2002; Romero-Viana *et al.* 2008). The increasing Ba_{bio} content indicates an enhancement in primary productivity, and the OM changes from type-III–II kerogen to type-II kerogen, suggesting an increase in planktonic algae content (Fig. 6a; Tribovillard *et al.* 2004; Liu & Wang, 2013). Planktonic algae use free CO_2 and HCO_3^- for photosynthesis, forming CO_3^{2-} (Fig. 15; Felfoldy, 1960; Han *et al.* 2018) and secreting calcium carbonate (Robbins & Blaekwelder, 1992; Hodell *et al.* 1998; Singh *et al.* 2017). Favourable chemical conditions of water body and biological processes together contribute to carbonate enrichment in this interval, corresponding to chemically and biochemically derived carbonate, respectively. This enrichment process of carbonate can be indirectly suggested by the negative correlations of carbonate content with the terrigenous clay minerals and quartz, as shown in Figure b–c.

CDS (Interval III): The lower ratios of Na/Al, Sr/Ba and Th/U indicate that the climate was warmer and wetter than during interval II, which brings a large volume of fresh water into the lake, leading to a further deepening of the water body as well as a decrease in salinity (Fig. 14). These conditions are not conducive to the chemical precipitation of carbonate (Romero-Viana *et al.* 2008). However, in this interval, milder temperatures enhance the lake

https://doi.org/10.1017/S0016756822000103 Published online by Cambridge University Press

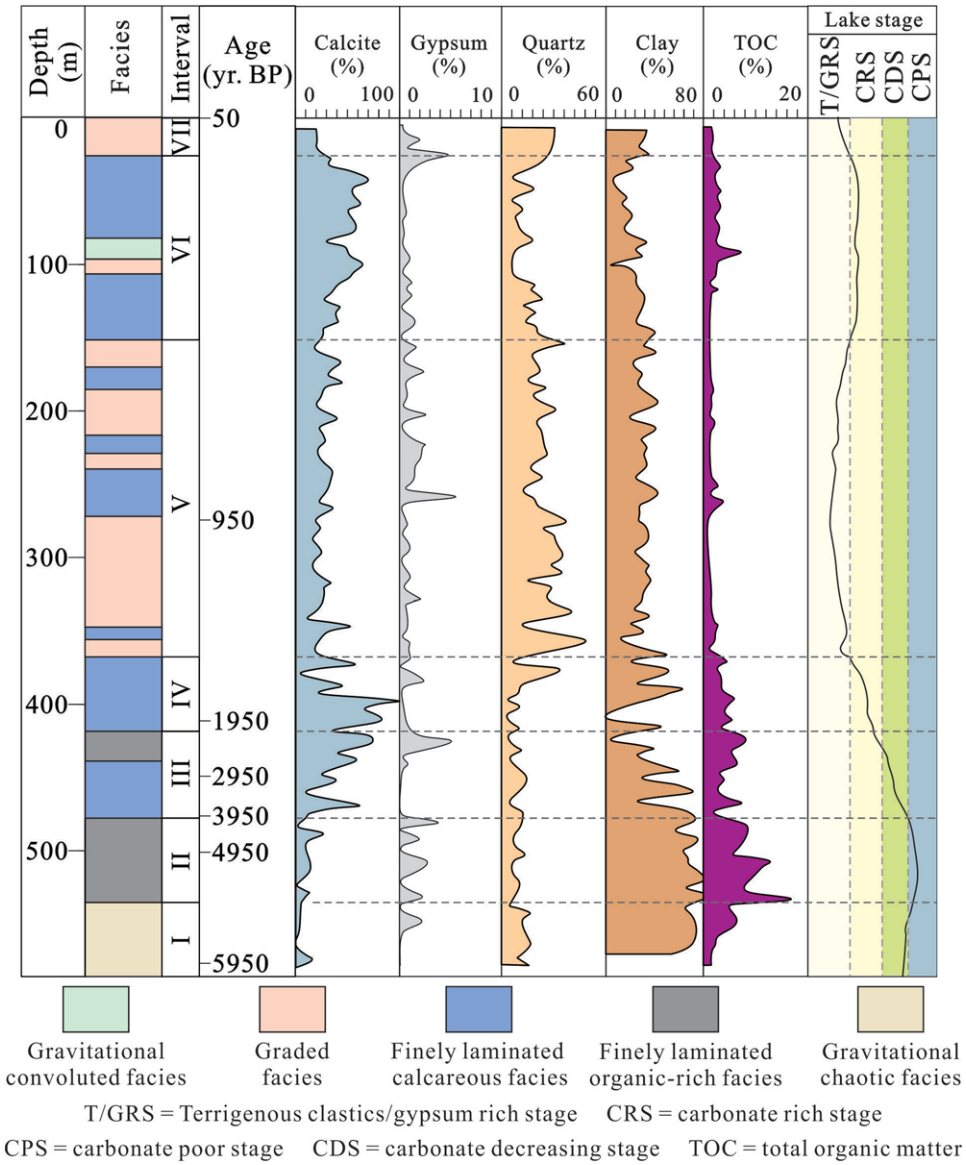

Fig. 12. (Colour online) Contents of sediments in 1A and 4A in Montcortès Lake, modified from Valero-Garcés *et al.* (2014).

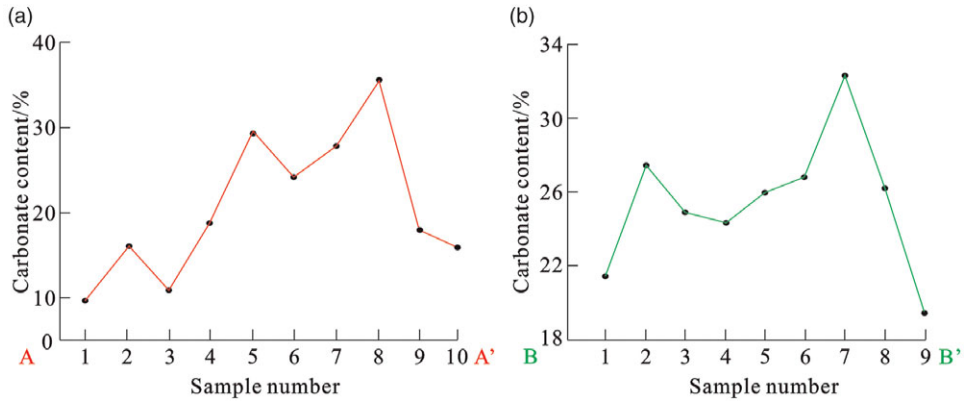

Fig. 13. (Colour online) Distribution of the Holocene lacustrine carbonates in AA′ (a) and BB′ (b) in Barkol Lake, modified from Zhao *et al.* (2010).

productivity, and the OM is dominated by type-II kerogen with more planktonic algae (Fig. 6a), which favour the biochemical precipitation of carbonate (Roeser *et al.* 2016). Compared with interval II, even though biochemically derived carbonate increases, chemically derived carbonate decreases, leading to a decrease in total carbonate.

CPS (Interval IV): The warmest and wettest climate leads to high primary productivity, strong freshwater input and low

https://doi.org/10.1017/S0016756822000103 Published online by Cambridge University Press

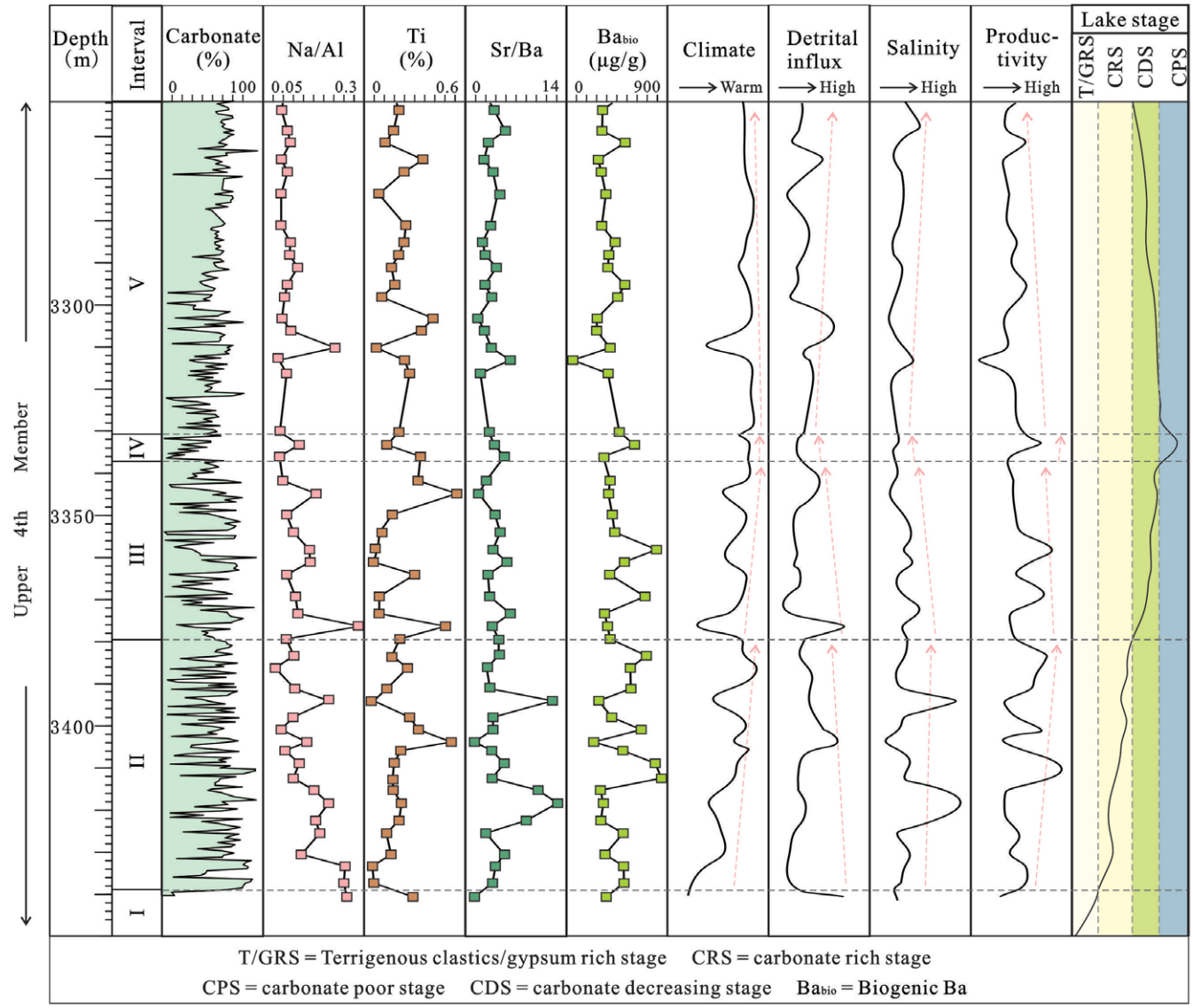

Fig. 14. (Colour online) Controlling factors of carbonate deposition in the Es4s sub-member in Well FY1.

salinity, inferred from the lowest ratios of Na/Al and Sr/Ba and the highest ratio of V/(V + Ni). The chemical precipitation of carbonate continues to decrease. In addition, a thermal stratification of the water body can be formed under this climate condition (Wagner & Adrian, 2011), reducing the mixing of water and material between the upper and lower layers in the lake (O'Reilly *et al.* 2003; Stainsby *et al.* 2011). The dissolved oxygen in the surface water does not easily penetrate to the bottom of the lake, resulting in a long-term anoxic condition that favours OM enrichment (Jankowski *et al.* 2006). The degradation of OM at the water bottom produces CO_2 and organic acid, affording a decrease in water pH and carbonate dissolution (Fig. 15; Emerson & Berder, 1981; Milliman *et al.* 1999; Mercedes-Martín *et al.* 2016). A relatively reduced carbonate supply and increased carbonate dissolution lead to the formation of the CPS.

Interval V: A considerably decreased V/(V + Ni) ratio and increased Th/U ratio indicate a reduction in the water depth. The salinity of the water body is similar to that of interval III (Fig. 14). The OM is dominated by type-II and type-II–III kerogen and is associated with relatively high primary productivity. Due to the effects of biology and biochemistry, carbonate is relatively enriched again.

A lake is a complex and varied dynamic system, in which detrital influx, climate, primary productivity and salinity all influence carbonate precipitation and dissolution, resulting in a variation in carbonate.

5.c. Formation conditions of VPC developed in this study

As demonstrated by the analysis of the Holocene carbonate deposition in modern lakes, the development of VPC in the Dongying Depression requires certain conditions, including but not limited to the following. (1) Sufficient carbonate from the weathering of the carbonate-rich provenance and calcareous organisms. (2) A particular water depth to ensure that light can penetrate for photosynthesis to facilitate carbonate precipitation, and to limit the effect of wind mixing, i.e. free from the exchange of the upper and lower water bodies (Schubel & Lowenstein, 1997; Quijada *et al.* 2013). For example, the maximum water depth is only *c.* 4–5 m in interval III at the Oro Lake (Fig. 11, Last &

https://doi.org/10.1017/S0016756822000103 Published online by Cambridge University Press

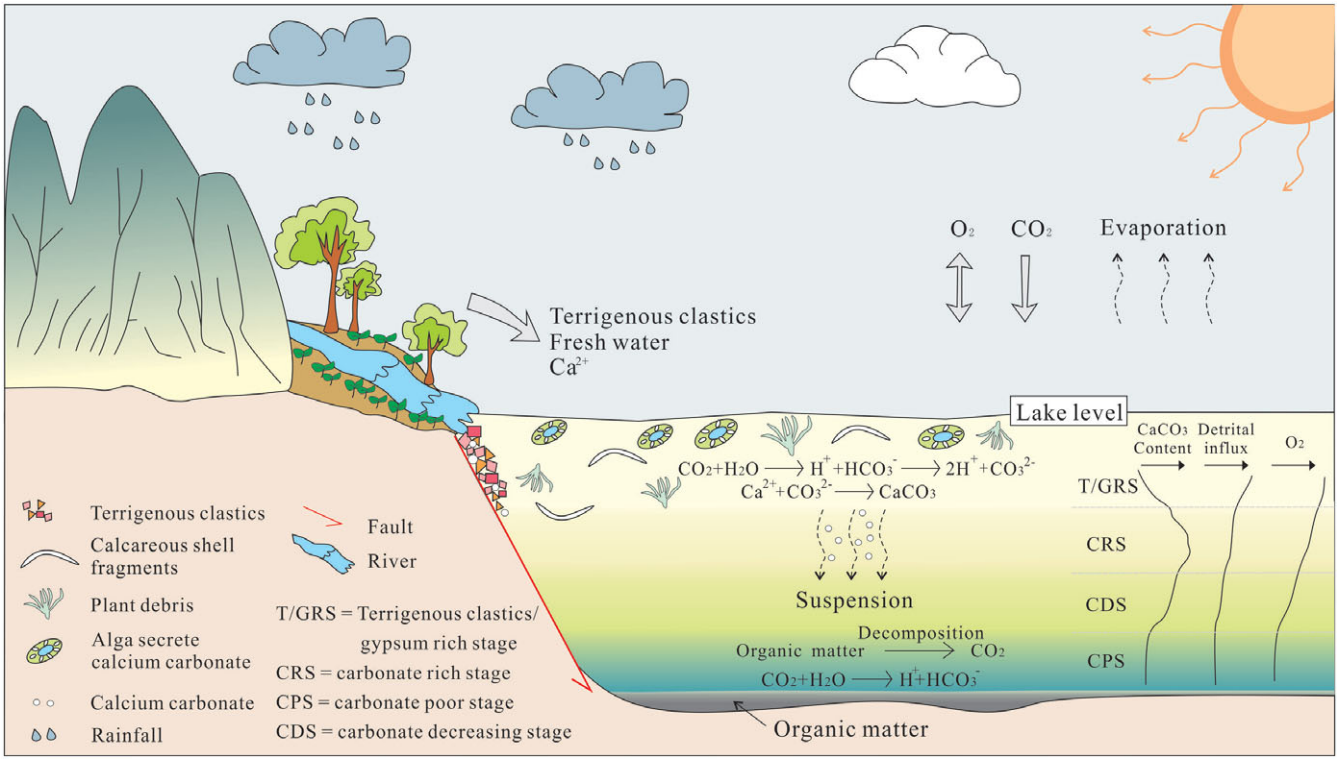

Fig. 15. (Colour online) Depositional model of the Es4s sub-member in the Dongying Depression.

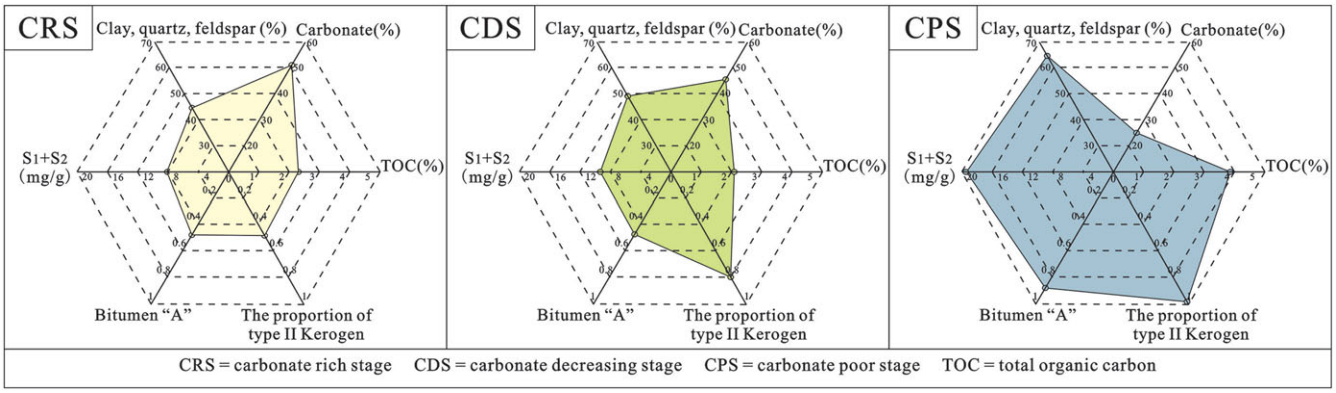

Fig. 16. (Colour online) The parameters of the CRS, CDS and CPS of the Es4s sub-member in the Dongying Depression.

Vance, 2002) and the carbonate content decreases mildly in the carbonate-decreasing stage. The carbonate-poor stage (CPS) is absent with the lack of sufficient water depth, which is different from the Dongying Depression. (3) Appropriate salinity is helpful to the formation of the carbonate-rich stage. For example, in the hypersaline Dead Sea, the carbonate precipitates mainly during a period of high water level, whereas during a period of shallow water the salinity increases, and gypsum and halite become the dominant precipitating minerals (Golan *et al.* 2017). (4) A closed lake will increase salinity and promote the formation of thermodynamic stratification, which result in an anoxic condition at the lake bottom (Liang *et al.* 2018b) that is helpful for OM enrichment. As mentioned above, the degradation of abundant OM acts as a crucial factor for the development of CPS in lakes. When the integrated conditions of the lake are appropriate, VPC similar to those in the Dongying Depression can appear in lakes Qinghai, Barkol and Montcortès.

5.d. Influence of carbonate variation

Organic matter enrichment, which is important to petroleum resources, is different in the distinct lake stages. The average TOC content is 2.3 wt % in the carbonate-rich stage (CRS), whereas it is 2.1 wt % in the carbonate-decreasing stage (CDS), with a higher average value of S1 + S2 (Fig. 16). The content of TOC, S1 + S2, and bitumen 'A' is highest in the carbonate-poor stage (CPS). The heterogeneous distribution of organic geochemical parameters is attributable to the different sedimentary conditions of the lake stages. The primary productivity is low, and oxygen content is relatively high, leading to poor conditions for OM preservation in the

https://doi.org/10.1017/S0016756822000103 Published online by Cambridge University Press

CRS (Figs 14 and 15), which makes OM accumulation difficult (Schieber, 2011). Both primary productivity and reducibility increase in the CDS. The proportion of type-II kerogen increases from 50 % in the CRS to 80 %, and the hydrocarbon generation efficiency of OM increases, resulting in more OM turning into S1 and S2 (Fig. 16). The primary productivity is high, and the preservation conditions for OM are favourable, with low oxygen content in the CPS (Stow *et al.* 2001). This is the optimal interval for OM enrichment. In addition, carbonate deposition, which influences the heterogeneous enrichment of OM, further affects the variation in carbonate crystal forms (from micritic to sparry calcite) as a result of organic–inorganic interactions during the thermal evolution of OM, particularly in the lamina-developed lithofacies (Liang *et al.* 2018*a*).

6. Conclusions

Four evolutionary stages were identified in the Eocene carbonate-rich Dongying Depression (China). During the terrigenous clastic / gypsum-rich stage, carbonates hardly precipitate owing to the influence of silty/gypseous sediments. During the carbonate-rich stage, large amounts of chemically and biochemically derived carbonate precipitate as the water body deepens. During the carbonate-decreasing stage, the continuous deepening and reduced salinity of the water body affected by a warm and humid climate yield a decrease in chemically derived carbonate. During the carbonate-poor stage, the degradation of organic matter promotes carbonate dissolution in the deep part of the lake. Similar varying patterns of carbonates (VPC) are observed in four Holocene lakes (the Qinghai Lake and Barkol Lake in China, Oro Lake in Canada, and Montcortès Lake in Spain). The development of VPC in the Dongying Depression requires certain conditions, including but not limited to a sufficient carbonate source, a particular water depth, an appropriate salinity and a relatively closed lake. A depositional model of carbonates in the Dongying Depression is developed based on the comparison of VPC in ancient and modern lakes. The findings of this study deepen the understanding of the diversity and genetic mechanisms of lacustrine carbonates.

Acknowledgements. The results discussed in this paper were supported by the Natural Science Foundation of Shandong Province (No. ZR2019BD042), the National Natural Science Foundation of China (No. 42072164, No. U1762217, No. 41902134 and No. 42172165), the Taishan Scholars Program (No. TSQN201812030), the Fundamental Research Funds for the Central Universities (19CX07003A) and the China Postdoctoral Science Foundation Grant (No. 2019M652435 and No. 2020T130384). Our deepest gratitude goes to Editor-in-Chief Peter Clift, Associate Editor J. Le Goff, reviewer C. Ian and an anonymous reviewer, and Editor Susie Cox and Susie Bloor for their excellent work and thoughtful suggestions that have helped to improve this manuscript considerably.

Declaration of Interest. None.

References

Algeo TJ and Ingall E (2007) Sedimentary Corg: P ratios, paleocean ventilation, and Phanerozoic atmospheric pO_2. *Palaeogeography, Palaeoclimatology, Palaeoecology* **256**, 130–55.

An ZS, Colman SM, Zhou WJ, Li XQ, Brown ET, Timothy Jull AJ, Cai YJ, Huang YS, Lu XF, Chang H, Song YG, Sun YB, Xu H, Liu WG, Jin ZD, Liu XD, Cheng P, Liu Y, Ai L, Li XZ, Liu XJ, Yan LB, Shi ZG, Wang XL, Wu F, Qiang XK, Dong JB, Lu FY and Xu XW (2012) Interplay between the westerlies and Asian monsoon recorded in Lake Qinghai sediments since 32 ka. *Scientific Reports* **2**, 619.

Aplin AC (1993) The composition of authigenic clay minerals in recent sediments: links to the supply of unstable reactants. In *Geochemistry of Clay-Pore Fluid Interactions* (eds DAC Manning, PL Hall and CR Hughes), pp. 81–106. London: Chapman & Hall.

Archer D, Emerson S and Reimers C (1989) Dissolution of calcite in deep-sea sediments: pH and O_2 microelectrode results. *Geochimica et Cosmochimica Acta* **53**, 2831–45.

Arthur MA and Sageman BB (1994) Marine black shales: depositional mechanisms and environments of ancient deposits. *Annual Review of Earth and Planetary Sciences* **22**, 449–551.

Bai CY, Yu BS, Liu HM, Xie ZH, Han SJ, Zhang LY, Ye RC and Ge J (2018) The genesis and evolution of carbonate minerals in shale oil formations from Dongying depression, Bohai Bay Basin, China. *International Journal of Coal Geology* **189**, 8–26.

Bassetti MA, Manzi V, Lugli S, Roveri M, Longinelli A, Lucchi FR and Barbieri M (2004) Paleoenvironmental significance of Messinian post-evaporitic lacustrine carbonates in the northern Apennines, Italy. *Sedimentary Geology* **172**, 1–18.

Bomou B, Adatte T, Tantawy AA, Mort H, Fleitmann D, Huang Y and Föllmi KB (2013) The expression of the Cenomanian–Turonian oceanic anoxic event in Tibet. *Palaeogeography, Palaeoclimatology, Palaeoecology* **369**, 466–81.

Chen ZH, Jiang WB, Zhang LY and Zha M (2018) Organic matter, mineral composition, pore size, and gas sorption capacity of lacustrine mudstones: implications for the shale oil and gas exploration in the Dongying depression, eastern China. *AAPG Bulletin* **102**, 1565–600.

Corella JP, Brauer A, Mangili C, Rull V, Vegas-Vilarrúbia T, Morellón M and Valero-Garcés BL (2012) The 1.5-ka varved record of Lake Montcortès (southern Pyrenees, NE Spain). *Quaternary Research* **78**, 323–32.

Corella JP, Moreno A, Morellón M, Rull V, Giralt S, Rico MT, Pérez-Sanz A and Valero-Garcés BL (2011) Climate and human impact on ameromictic lake during the last 6000 years (Montcortès Lake, Central Pyrenees, Spain). *Journal of Paleolimnology* **46**, 351–67.

Davies SJ and Elliot T (1996) Spectral gamma ray characterization of high resolution sequence stratigraphy: examples from Upper Carboniferous fluvio-deltaic systems, County Clare, Ireland. In *High Resolution Sequence Stratigraphy: Innovations and Applications* (eds JA Howell and JF Aitken), pp. 25–35. Geological Society of London, Special Publication no. 104,.

Dean WE (1999) The carbon cycle and biogeochemical dynamics in lake sediments. *Journal of Paleolimnology* **21**, 375–93.

Dean WE and Megard RO (1993) Environment of deposition of CaCO3 in Elk Lake, Minnesota. In *Elk Lake, Minnesota: Evidence for Rapid Climate Change in the North-Central United States* (eds JP Bradbury and WE Dean), pp. 97–114. Geological Society of America, Special Paper 276.

Détriché S, Bréhéret JG, Karrat L, Hinschberger F and Macaire JJ (2013) Environmental controls on the Late Holocene carbonate sedimentation of a karstic lake in the Middle-Atlas Mountains (Lake Afourgagh, Morocco). *Sedimentology* **60**, 1231–56.

Ding F, Zhang JL, Xie J, Li CL, Shi CQ, Zhang PH, Zhang M and Tang MM (2014) Fine description of structure and sedimentary microfacies of Li32 block of Lijin oilfield, Dongying depression, China. *Arabian Journal of Geosciences* **7**, 1693–704.

Dymond J, Suess E and Lyle M (1992) Barium in deep-sea sediments: a geochemical proxy for paleoproductivity. *Paleoceanography* **7**, 163–81.

Einsele G, Yan JP and Hinderer M (2001) Atmospheric carbon burial in modern lake basins and its significance for the global carbon budget. *Global and Planetary Change* **30**, 167–95.

Emerson S and Berder M (1981) Carbon fluxes at the sediment/water interface of the deep sea: calcium carbonate preservation. *Journal of Marine Research* **39**, 139–62.

Felfoldy L (1960) Experiments on the carbonate assimilation of some unicellular algae by Ruttner's conductometric method. *Acta Biologica Hungarica* **11**, 67–75.

Feng YL, Li ST and Lu YC (2013) Sequence stratigraphy and architectural variability in Late Eocene lacustrine strata of the Dongying Depression, Bohai Bay Basin, Eastern China. *Sedimentary Geology* **295**, 1–26.

https://doi.org/10.1017/S0016756822000103 Published online by Cambridge University Press

Gierlowski-Kordesch EH (2010) Lacustrine carbonates. In *Carbonates in Continental Settings: Facies, Environments, and Processes* (eds AM Alonso-Zarza and LH Tanner), pp. 1–101. Amsterdam: Elsevier.

Gilbert R and Leask SM (1981) Factors affecting marl deposition in Knowlton Lake, Southeastern Ontario. *Journal of Great Lakes Research* **7**, 286–9.

Golan R, Lazar B, Wurgaft E, Lensky N, Ganor J and Gavrieli I (2017) Continuous CO_2 escape from the hypersaline Dead Sea caused by aragonite precipitation. *Geochimica et Cosmochimica Acta* **207**, 43–56.

Guo XW, He S, Liu KY, Song GQ, Wang XJ and Shi ZS (2010) Oil generation as the dominant overpressure mechanism in the Cenozoic Dongying depression, Bohai Bay Basin, China. *AAPG Bulletin* **94**, 1859–81.

Han ZZ, Yu WW, Zhao H, Zhao YH, Tucker M E and Yan HX (2018) The significant roles of Mg/Ca ratio, Cl^- and SO_4^{2-} in carbonate mineral precipitation by the halophile Staphylococcus epidermis Y2. *Minerals* **8**, 1–25.

Hodell DA, Brenner M, Kanfoush SL, Curtis JH, Stoner JS, Song XL, Wu Y and Whitmore TJ (1999) Paleoclimate of Southwestern China for the past 50,000 yr inferred from lake sediment records. *Quaternary Research* **52**, 369–80.

Hodell DA, Sehelske CL, Fahnenstiel GL and Robbins LL (1998) Biologically induced calcite and its isotopic composition in Lake Ontario. *Limnology and Oceanography* **43**, 187–99.

Huang DF (1981) Characteristics and geochemical significance of organic material in the sediments of modern lakes. *Geology Geochemistry* **5**, 25–36 (in Chinese).

Jankowski T, Livingstone DM, Bührer H, Forster R and Niederhauser P (2006) Consequences of the 2003 European heat wave for lake temperature profiles, thermal stability, and hypolimnetic oxygen depletion: implications for a warmer world. *Limnology and Oceanography* **51**, 815–9.

Jiang ZX, Chen DZ, Qiu LW, Liang HB and Ma J (2007) Source-controlled carbonates in a small Eocenehalf–grabenbasin (Shulu Sag) in central Hebei Province, North China. *Sedimentology* **54**, 265–92.

Jiang ZX, Liu H, Zhang SW, Su X and Jiang ZL (2011) Sedimentary characteristics of large-scale lacustrine beach-bars and their formation in the Eocene Boxing Sag of Bohai Bay Basin, East China. *Sedimentology* **58**, 1087–112.

Katz BJ (2001) Lacustrine basin hydrocarbon exploration: current thoughts. *Journal of Paleolimnology* **26**, 161–79.

Kong XX, Jiang ZX, Han C, Zheng LJ, Zhang YM, Zhang RF and Tian JZ (2017) Genesis and implications of the composition and sedimentary structure of fine-grained carbonate rocks in the Shulu sag. *Journal of Earth Science* **28**, 1047–63.

Last FM and Last WM (2012) Lacustrine carbonates of the northern Great Plains of Canada. *Sedimentary Geology* **277–278**, 1–31.

Last WM and Vance RE (2002) The Holocene history of Oro Lake, one of Western Canada's longest continuous lacustrine records. *Sedimentary Geology* **148**, 161–84.

Lettéron A, Hamon Y, Fournier F, Séranne M, Pellenard P and Joseph P (2018) Reconstruction of a saline, lacustrine carbonate system (Priabonian, St-Chaptes Basin, SE France): depositional models, paleogeographic and paleoclimatic implications. *Sedimentary Geology* **367**, 20–47.

Li FL and Li WS (2017) Petrological record of CO_2 influx in the Dongying Sag, Bohai Bay Basin, NE China. *Applied Geochemistry* **84**, 373–86.

Li MW, Chen ZH, Ma XX, Cao TT, Li ZM and Jiang QG (2018) A numerical method for calculating total oil yield using a single routine Rock-Eval program: a case study of the Eocene Shahejie Formation in Dongying Depression, Bohai Bay Basin, China. *International Journal of Coal Geology* **191**, 49–65.

Li Y, Wang NA, Li ZL, Zhou XH, Zhang CQ and Wang Y (2013) Carbonate formation and water level changes in a paleo-lake and its implication for carbon cycle and climate change,arid China. *Frontiers of Earth Science* **7**, 487–500.

Li ZF, Lv YB, Tao SC and An CB (2008) Holocene climate changes in eastern Xinjiang: a case study on Barkol Lake. *Marine Geology and Quaternary Geology* **28**, 107–12 (in Chinese with English abstract).

Li ZX, Yang W, Wang YS, Zhang LQ, Luo HM, Liu SH, Zhang LK and Luo XR (2019) Anatomy of a lacustrine stratigraphic sequence within the fourth member of the Eocene Shahejie Formation along the steep margin of the Dongying depression, eastern China. *AAPG Bulletin* **103**, 469–504.

Liang C, Cao Y, Jiang Z, Wu J, Song G and Wang Y (2017) Shale oil potential of lacustrine black shale in the Eocene Dongying depression: implications for geochemistry and reservoir characteristics. *AAPG Bulletin* **101**, 1835–58.

Liang C, Cao YC, Liu KY, Jiang Z, Wu J and Hao F (2018a) Diagenetic variation at the lamina scale in lacustrine organic-rich shales: implications for hydrocarbon migration and accumulation. *Geochimica et Cosmochimica Acta* **229**, 112–28.

Liang C, Jiang Z, Cao Y, Wu J, Wang Y and Fang H (2018b) Sedimentary characteristics and origin of lacustrine organic-rich shale in the salinized Eocene Dongying Depression. *GSA Bulletin* **130**, 154–74.

Lima BEM and Ros LFD (2019) Deposition, diagenetic and hydrothermal processes in the Aptian Pre-Salt lacustrine carbonate reservoirs of the northern Campos Basin, offshore Brazil. *Sedimentary Geology* **383**, 55–81.

Liu CL and Wang PX (2013) The role of algal blooms in the formation of lacustrine petroleum source rocks: evidence from Jiyang depression, Bohai Gulf Rift Basin, eastern China. *Palaeogeography, Palaeoclimatology, Palaeoecology* **388**, 15–22.

Liu HM, Zhang S, Song GQ, Zhang SP, Hao XF, Xie ZH, Xu NN and Liu P (2017) A discussion on the origin of shale reservoir inter-laminar fractures in the Shahejie Formation of Paleogene, Dongying depression. *Journal of Earth Science* **28**, 1064–77.

Liu WG, Liu H, Wang Z, An ZS and Cao YN (2017) Hydrogen isotopic compositions of long-chain leaf wax n-alkanes in Lake Qinghai sediments record palaeohydrological variations during the past 12 ka. *Quaternary International* **449**, 67–74.

Liu WG, Zhang PJ, Zhao C, Wang HY, An ZS and Liu H (2018) Reevaluation of carbonate concentration and oxygen isotope records from Lake Qinghai, the northeastern Tibetan Plateau. *Quaternary International* **482**, 122–30.

Loucks RG and Stephen CR (2007) Mississippian Barnett Shale: lithofacies and depositional setting of a deep-water shale-gas succession in the Fort Worth Basin, Texas. *AAPG Bulletin* **91**, 579–601.

Ma YQ, Fan MJ, Lu YC, Liu HM, Hao YQ, Xie ZH, Liu ZH, Peng L, Du XB and Hu HY (2016) Climate-driven paleolimnological change controls lacustrine mudstone depositional process and organic matter accumulation: constraints from lithofacies and geochemical studies in the Zhanhua Depression, eastern China. *International Journal of Coal Geology* **167**, 103–18.

Macquaker JHS and Adams AE (2003) Maximizing information from fine-grained sedimentary rocks: an inclusive nomenclature for mudstones. *Journal of Sedimentary Research* **73**, 735–44.

Mercedes-Martín R, Rogerson MR, Brasier AT, Vonhof HB, Prior TJ, Fellows SM, Reijmer JJG, Billing I and Pedley HM (2016) Growing spherulitic calcite grains in saline, hyperalkaline lakes: experimental evaluation of the effects of Mg-clays and organic acids. *Sedimentary Geology* **335**, 93–102.

Milliman JD, Troy PJ, Balch WM, Adams AK, Li YH and Mackenzie FT (1999) Biologically mediated dissolution of calcium carbonate above the chemical lysocline? *Deep-Sea Research* **46**, 1653–69.

Montero-Serrano JC, Föllmi KB, Adatte T, Spangenberg JE, Tribovillard N, Fantasia A and Suan G (2015) Continental weathering and redox conditions during the early Toarcian oceanic anoxic event in the northwestern Tethys: insight from the Posidonia shale section in the Swiss Jura Mountains. *Palaeogeography, Palaeoclimatology, Palaeoecology* **429**, 83–99. https://www.sciencedirect.com/science/article/abs/pii/S0031018215001832?via%3Dihub

Murphy AE, Sageman BB, Hollander DJ, Lyons TL and Brett CE (2000) Black shale deposition and faunal overturn in the Devonian Appalachian Basin: clastic starvation, seasonal water-column mixing, and efficient biolimiting nutrient recycling. *Paleoceanography* **15**, 280–91.

Nelson ST and Rey KA (2018) Multi-proxy reassessment of the paleolimnology of Lake Bonneville (western USA) as observed in the restricted Pilot Valley sub-basin. *Journal of Quaternary Science* **33**, 177–93.

O'Reilly CM, Alin SR, Plisnier PD, Cohen AS and McKee BA (2003) Climate change decreases aquatic ecosystem productivity of Lake Tanganyika, Africa. *Nature* **424**, 766–8.

Platt NH and Wright VP (1991) Lacustrine carbonate facies models, facies distributions and hydrocarbon aspects. In *Lacustrine Facies Analysis* (eds. P Anadon, L Cabrera and K Kelts), pp. 57–74. International Association of Sedimentologists (IAS) Special Publication 13. Oxford: Blackwell Scientific Publications.

https://doi.org/10.1017/S0016756822000103 Published online by Cambridge University Press

Qian LB and Song YG (2010) Mineralogical records of hole 1F in lake Qinghai and their paleoclimatic implications. *Marine Geology and Quaternary Geology* **30**, 107–14 (in Chinese with English abstract).

Quijada IE, Suarez-Gonzalez P, Benito MI and Mas R (2013) Depositional depth of laminated carbonate deposits: insights from the Lower Cretaceous Valdeprado formation (Cameros Basin, Northern Spain). *Journal of Sedimentary Research* **83**, 241–57.

Robbins LL and Blaekwelder PL (1992) Biochemical and ultrastructural evidence for the origin of whitings: a biologically induced calcium carbonate precipitation mechanism. *Geology* **20**, 464–8.

Roeser P, Franz SO and Litt T (2016) Aragonite and calcite preservation in sediments from Lake Iznik related to bottom lake oxygenation and water column depth. *Sedimentology* **63**, 2253–77.

Romero-Viana L, Julia R, Camacho A, Vicente E and Miracle MR (2008) Climate signal in varve thickness: Lake LaCruz (Spain), a case study. *Journal of Paleolimnology* **40**, 703–14.

Schieber J (2011) Marcasite in black shales: a mineral proxy for oxygenated bottom waters and intermittent oxidation of carbonaceous muds. *Journal of Sedimentary Research* **81**, 447–58.

Schrag DP, Higgins JA, Macdonald FA and Johnston DT (2013) Authigenic carbonate and the history of the global carbon cycle. *Science* **339**, 540–3.

Schubel KA and Lowenstein TK (1997) Criteria for the recognition of shallow-perennial-saline-lake halites based on recent sediments from the Qaidam Basin, western China. *Journal of Sedimentary Research* **67**, 74–87.

Shapley MD, Ito E and Donovan JJ (2005) Authigenic calcium carbonate flux in groundwater-controlled lakes: implications for lacustrine paleoclimate records. *Geochimica et Cosmochimica Acta* **69**, 2517–33.

Singh DP, Saraswat R, Naik DK and Nigam R (2017) A first look at factors affecting aragonite compensation depth in the eastern Arabian Sea. *Palaeogeography, Palaeoclimatology, Palaeoecology* **483**, 6–14.

Slatt RM and Rodriguez ND (2012) Comparative sequence stratigraphy and organic geochemistry of gas shales: commonality or coincidence? *Journal of Natural Gas Science and Engineering* **8**, 68–84.

Stainsby EA, Winter JG, Jarjanazi H, Paterson AM, Evans DO and Young JD (2011) Changes in the thermal stability of Lake Simcoe from 1980 to 2008. *Journal of Great Lakes Research* **37**, 55–62.

Stephenson MH, Leng MJ, Michie U and Vane CH (2006) Palaeolimnology of Palaeozoic lakes, focussing on a single lake cycle in the Middle Devonian of the Orcadian Basin, Scotland. *Earth-Science Reviews* **75**, 177–97.

Stow DAV, Hue AY and Bertrand P (2001) Depositional processes of black shale in deep water. *Marine and Petroleum Geology* **18**, 491–8.

Su X, Ding X, Jiang ZX, Hu B, Meng MC and Chen MS (2012) Using of multi-microfossil proxies for reconstructing quantitative of paleo-water depth during the deposit period of LST of Es4s in Dongying Depression. *Earth Science Frontiers* **19**, 188–99 (in Chinese with English abstract).

Talbot MR and Kelts K (1986) Primary and diagenetic carbonates in the anoxic sediments of Lake Bosumtwi, Ghana. *Geology* **14**, 912–6.

Thompson DL, Stilwell JD and Hall M (2015) Lacustrine carbonate reservoirs from Early Cretaceous rift lakes of Western Gondwana: Pre-Salt coquinas of Brazil and West Africa. *Gondwana Research* **28**, 26–51.

Tian JJ and Jiang ZX (2009) Sequence stratigraphy characteristics and sedimentary system evolution of Upper Es4 in the Dongying Depression. *Acta Geologica Sinica* **83**, 88–98 (in Chinese with English abstract).

Tribovillard N, Algeo TJ, Lyons T and Riboulleau A (2006) Trace metals as paleoredox and paleoproductivity proxies: an update. *Chemical Geology* **232**, 12–32.

Tribovillard N, Riboulleau A, Lyons T and Baudin F (2004) Enhanced trapping of molybdenum by sulfurized organic matter of marine origin as recorded by various Mesozoic formations. *Chemical Geology* **213**, 385–401.

Valero-Garcés B, Morellón M, Moreno A, Corella JP, Martín-Puertas C, Barreiro F, Pérez A, Giralt S and Mata-Campo MP (2014) Lacustrine carbonates of Iberian Karst Lakes: sources, processes and depositional environments. *Sedimentary Geology* **299**, 1–29.

Wagner C and Adrian R (2011) Consequences of changes in thermal regime for plankton diversity and trait composition in a polymictic lake: a matter of temporal scale. *Freshwater Biology* **56**, 1949–61.

Xu H, Ai L, Tan LC and An ZS (2006) Stable isotopes in bulk carbonates and organic matter in recent sediments of Lake Qinghai and their climatic implications. *Chemical Geology* **235**, 262–75.

Xu H, Liu XY, An ZS, Hou ZH, Dong JB and Liu B (2010) Spatial pattern of modern sedimentation rate of Qinghai Lake and a preliminary estimate of the sediment flux. *Chinese Science Bulletin* **55**, 621–7.

Yang T, Cao YC, Friis H, Wang YZ and Zhou LL (2018) Diagenetic evolution and chemical changes of deep-water mudstones of Shahejie Formation in the Dongying Sag, Jiyang Depression, Eastern China. *Marine and Petroleum Geology* **93**, 14–32.

Yu JQ and Kelts KR (2002) Abrupt changes in climatic conditions across the late-glacial/Holocene transition on the NE Tibet–Qinghai Plateau: evidence from Lake Qinghai, China. *Journal of Paleolimnology* **28**, 195–206.

Zahid MA, Chunmei D, Lin C, Gluyas J, Jones S, Zhang X, Munawar MJ and Ma C (2016) Sequence stratigraphy, sedimentary facies and reservoir quality of Es4s, southern slope of Dongying Depression, Bohai Bay Basin, East China. *Marine and Petroleum Geology* **77**, 448–70.

Zeng MX, Song YG, An ZS, Chang H and Li Y (2014) Clay mineral records of the Erlangjian drill core sediments from the Lake Qinghai Basin, China. *Science China Earth Sciences* **57**, 1846–59.

Zhang JG, Jiang ZX, Liang C, Wu J, Xian BZ and Li Q (2016) Lacustrine massive mudrock in the Eocene Jiyang Depression, Bohai Bay Basin, China: nature, origin and significance. *Marine and Petroleum Geology* **77**, 1042–55.

Zhang YF, Yuan XD, Wang M, Ge PC, Huo YC, Xu J, Zhang JG, Cheng J and Jiang ZX (2021) Discovery of lacustrine shale deposits in the Yanshan Orogenic Belt, China: implications for hydrocarbon exploration. *Geoscience Frontiers* **12**, 101256. doi: 10.1016/j.gsf.2021.101256.

Zhao JJ, Lv YB, An CB, Tao SC, Zheng TM and Dong WM (2010) Carbonates in lacustrine sediments of lake Balikun, Xinjiang, China. *Marine Geology and Quaternary Geology* **30**, 125–31(in Chinese with English abstract).

Zhong W, Pen ZH, Xue JB, Ouyang J, Tang XH and Cao JY (2012) Geochemistry of sediments from Barkol Lake in the westerly influenced northeast Xinjiang: implications for catchment weathering intensity during the Holocene. *Journal of Asian Earth Sciences* **50**, 7–13.

Zou CN, Yang Z, Cui JW, Zhu RK, Hou LH, Tao SZ, Yuan XJ, Wu ST, Lin SH, Wang L, Bai B and Yao JL (2013) Formation mechanism, geological characteristics and development strategy of nonmarine shale oil in China. *Petroleum Exploration and Development* **40**, 15–27.